

Nested Deep Learning Model Towards a Foundation Model for Brain Signal Data

Fangyi Wei¹, Jiajie Mo², Kai Zhang², Haipeng Shen¹, Srikantan
Nagarajan³, and Fei Jiang^{*4}

¹Innovation and Information Management, Faculty of Business and
Economics, The University of Hong Kong, China

²Department of Neurosurgery, Beijing Tiantan Hospital, China

³Department of Radiology, University of California, San Francisco

⁴Department of Epidemiology and Biostatistics, University of California,
San Francisco

Abstract

Epilepsy affects around 50 million people globally. Electroencephalography (EEG) or Magnetoencephalography (MEG) based spike detection plays a crucial role in diagnosis and treatment. Manual spike identification is time-consuming and requires specialized training that further limits the number of qualified professionals. To ease the difficulty, various algorithmic approaches have been developed. However, the existing methods face challenges in handling varying channel configurations and in identifying the specific channels where the spikes originate. A novel Nested Deep Learning (NDL) framework is proposed to overcome these limitations. NDL applies a weighted combination of signals across all channels, ensuring adaptability to different channel setups, and allows clinicians to identify key channels more accurately. Through theoretical analysis and empirical validation on real EEG/MEG datasets, NDL is shown to improve prediction accuracy, achieve channel localization, support cross-modality data integration, and adapt to various neurophysiological applications.

Keywords: epilepsy, Electroencephalography, spike detection, deep learning, neuroimaging.

*Email: fei.jiang@ucsf.edu

1 Introduction

Currently, around 50 million people worldwide suffer from epilepsy, one of the most common neurological diseases globally (World Health Organization 2024). Detecting epileptiform discharges, particularly spikes, during the interictal periods, plays a crucial role in the diagnosis of epilepsy.

Spikes are abnormal brain activities that typically occur intermittently and spontaneously, lasting around 100 to 250 milliseconds, in epilepsy patients. They can be measured with Electroencephalography (EEG) or Magnetoencephalography (MEG) devices. The devices collect brain signals through EEG or MEG sensors attached to different areas of the scalp and visualize the signals as time series waveforms. The EEG or MEG recordings then consist of multi-channel time series signal data. Identifying spikes not only helps predict the risk of seizures, but also helps localize the onset zone of seizures, which is critical for epilepsy surgery (Smith et al. 2022).

Thus, it becomes imperative to develop novel interpretable methods that can effectively identify spikes to assist clinical decisions. However, clinical practices predominantly employ manual identification of spikes, which is a labor-intensive process, especially when analyzing continuous or video EEG studies that can last more than 24 hours. Furthermore, this task requires specialized training, restricting the number of clinicians qualified to evaluate EEG studies, resulting in a significant shortage of neurologists trained in interpreting EEG data (Torres and Butter 1996).

To mitigate this issue, various algorithm-based methods have been proposed to automate the identification process. Indiradevi et al. (2008) use wavelet transformation to decompose spike signals. Lodder et al. (2013) adopt template matching to compare signal

patterns with spike templates. Baud et al. (2018) use an unsupervised learning approach to automate spike detection. With the advancement of deep learning, the field has increasingly embraced deep learning algorithms for spike detection. For example, Antoniadou et al. (2016), Johansen et al. (2016), Tjepkema-Cloostermans et al. (2018), Thomas et al. (2020), Clarke et al. (2021), Chung et al. (2023) and Munia et al. (2023) employ convolutional neural networks (CNNs) to classify abnormal and normal waveforms; Medvedev et al. (2019) use a Long Short-Term Memory neural network for the spike detection task.

Despite these developments, two significant challenges remain. Firstly, different studies have varying numbers and locations of the channels, as well as the montages used, all of which make it difficult to develop a universal algorithm that can accommodate all channel setups. For instance, Golmohammadi et al. (2019) develop an algorithm based on spikes labeled using the temporal central parasagittal montage with 22 channels, whereas Jing et al. (2020)'s algorithm is designed for the longitudinal bipolar montage with 18 channels and the common average reference montage with 19 channels. A general adaptive algorithm is crucial because it allows data integration between studies, thereby enhancing prediction accuracy. It also allows clinicians to choose their preferred montage for analysis.

Secondly, although current detection algorithms can identify time segments that contain spikes, they lack the ability to pinpoint the exact channels where the spikes originate. Identifying specific channels is crucial because it helps locate the seizure onset zone, helps clinicians review and validate detection results, and serves as a key factor in ruling out false detections in less likely channels.

We propose a novel nested deep learning framework (NDL) to address these challenges. For the first challenge, we propose a weight function for each channel, customized to its specific signal pattern within a given time range of interest, preferably less than one second.

Then we model the probability of a time segment to contain a spike via a weighted combination of signals across all channels. For the second challenge, these weights are designed to reflect the importance of each channel in terms of its relevance in the spike detection.

Our NDL approach is superior to the traditional channel-based methods (Wilson et al. 1999; Goelz et al. 2000), which require the tedious process of labeling each channel to achieve similar results. NDL offers a faster inference process that can handle large volumes of data simultaneously. Furthermore, NDL considers the signal information from all channels, which improves the prediction accuracy because there are often concurrent spikes that appear on multiple channels. Moreover, because NDL is invariant to channel configurations, it can serve as a foundational model for integrating neurophysiological data from various modalities and can be fine-tuned to adapt to different new tasks.

We apply NDL to three real datasets to evaluate its performance in Section 5. We start with a well-labeled EEG dataset from Temple University Hospital (TUH), focusing on its sensitivity and specificity in detecting spikes, as well as its accuracy in identifying the EEG channels where these spikes occur (Section 5.1). The dataset is the only public EEG dataset that provides not only the time label of spike occurrence but also the specific channels containing the spikes, as the ground truth for the evaluation. We then apply NDL to two private datasets: a 140-channel MEG dataset from the University of California, San Francisco (UCSF), and a 19-channel EEG dataset from China’s Beijing Tiantan Hospital (BTH). The results first demonstrate that the model trained on the UCSF MEG data performs well in detecting spikes and identifying relevant channels (Section 5.2). Furthermore, the MEG-trained model can even successfully detect spikes in the out-of-sample BTH EEG data, even though the testing data modality differs from the training data modality (Section 5.3). This study indicates that NDL has strong generalizability across different

datasets, even with varying numbers of channels. Finally, Section 5.4 proposes an algorithm that enables the application of NDL to continuous MEG/EEG recordings commonly available in practice.

The rest of the paper is presented as follows. We introduce the three real datasets and their preprocessing procedures in Section 2. Then we introduce the model in Section 3, and present the deep learning estimation procedure and the asymptotic consistency in Section 4. Finally, we demonstrate the performance of NDL on the three real datasets and its comparison with existing methods in Section 5.

To facilitate the presentation, we define the following notations. The L_0 , L_1 , L_2 and the supremum norms of a vector \mathbf{v} are denoted by $\|\mathbf{v}\|_0$, $\|\mathbf{v}\|_1$, $\|\mathbf{v}\|_2$ and $\|\mathbf{v}\|_\infty$, respectively. Furthermore, for a given matrix \mathbf{M} , we denote the matrix entry-wise supremum norm, L_0 , L_1 , the operator norms as $\|\mathbf{M}\|_\infty$, $\|\mathbf{M}\|_0$, $\|\mathbf{M}\|_1$, and $\|\mathbf{M}\|_2$, respectively. For a function $f(\mathbf{x})$, we denote the functional supremum norm as $\|f(\mathbf{x})\|_\infty \equiv \sup |f(\mathbf{x})|$.

Note: The replication codes are provided: https://github.com/shirleyweify/NDL_Replication_Code.git. The open data model is made publicly available, whereas access to the private data model requires a formal request.

2 Three Real Datasets

2.1 TUH Dataset

The TUH dataset (Harati et al. 2015) is the only publicly available scalp interictal EEG dataset that includes per-channel annotations. The dataset consists of 511 continuous EEG records using the standard 10/20 channel configuration, collected from 370 patients. Each record is collected at a sampling frequency of 250 Hz. We filter the data and retain frequencies between 1 and 70 Hz to remove the slow wave and fast oscillations caused

by the artifacts and noise. Then we remove the linear trend of the data. The data are then transformed into the Temporal Central Parasagittal montage, as described in Lopez et al. (2016), using the 22 channels listed in Table S1 in the supplementary material. This montage was chosen because it had been used when labeling the data.

Each EEG record has one or more channel-specific one-second annotations. According to Obeid and Picone (2016), these annotations include six classes: (1) spike and sharp wave (SPSW), (2) generalized periodic epileptiform discharge (GPED), (3) periodic lateralized epileptiform discharge (PLED), (4) eye movement (EYEM), (5) artifact (ARTF), and (6) background (BCKG). Among the six classes, SPSW, GPED and PLED are abnormal events of clinical interest, while EYEM, ARTF and BCKG are artifacts and normal signals.

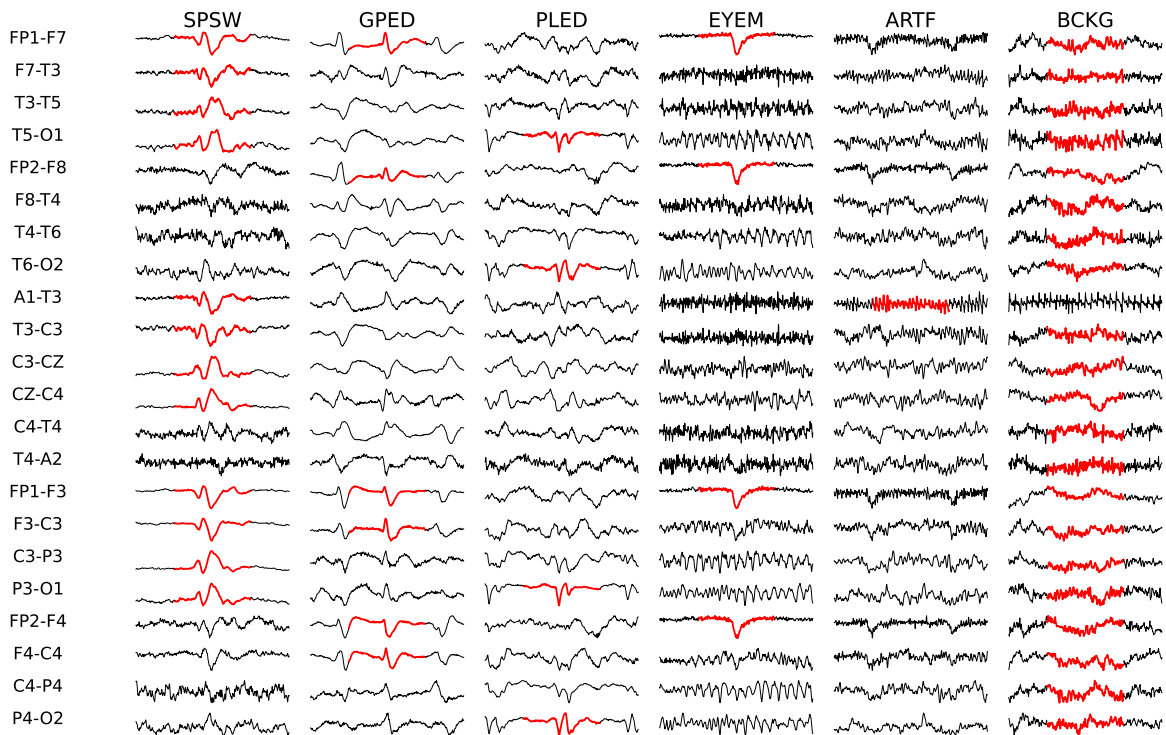


Figure 1: TUH: Two-second segments of the six classes of events with 22 ACNS TCP montages, where the one-second annotated events are shown in red and bold.

We extract a two-second segment around each annotation, where the middle one-second

segment is annotated, while the remaining is treated as background references. In total, we obtain 12,675 EEG segments from the TUH dataset. Figure 1 provides examples of the two-second segments for each class of the annotations. Table 1 reports the number of segments and the number of patients for each class.

Table 1: TUH: Numbers of segments and corresponding numbers of patients for each of the six classes, in both the training set and the testing set.

TUH Data		Abnormal			Normal		
		SPSW	GPED	PLED	EYEM	ARTF	BCKG
Training	# Segments	144	2607	2072	498	1587	3232
	# Patients	35	50	49	73	165	264
Testing	# Segments	41	616	516	146	371	845
	# Patients	23	49	46	49	123	236

2.2 UCSF MEG Dataset

The UCSF MEG data are recorded from 277 epilepsy patients who have undergone MEG tests at the MEG center of UCSF between 2019 and 2022. Each MEG recording has a labeling file stored on the clinical server. First, the recording is fully screened by a technologist to mark out candidate spikes. These candidate spikes are then reviewed by a clinician, often with 1 or 2 residents, to confirm the presence of the spikes. This process ensures that the spike labels are validated through multiple readers.

The MEG records are collected at a sampling frequency of 600 Hz on 140 channels. We filter the data to retain frequencies between 1 and 45 Hz, downsample the data to 256 Hz, and remove the linear trend of the data. Since the spike labels are less than 250 milliseconds, we extract a segment of 0.5 seconds around each label, where the middle 0.25-second

segment contains a spike annotation and the remaining signals are background references. We also extract 0.5-second background segments from non-spike-labeled time. These background segments can accurately represent non-spike activities. We obtain 230,325 segments, among which 46% are spike segments labeled in the clinical notes.

2.3 BTH EEG Dataset

The BTH EEG data are collected at China’s Beijing Tiantan Hospital, to test the adaptability of NDL across multi-modal data. The dataset consists of 84 EEG records with 19 channels, collected from 20 patients. In total, 53 spike events are annotated and confirmed by two trained clinicians. To increase the variability in background waveforms, we extract 50 subsets of background events from the normal periods. Each sub-dataset then consists of the 53 spike segments and another 53 randomly-selected background segments.

The raw data are collected at a sampling frequency of 512 Hz. We apply a filter to retain frequencies between 1 and 45 Hz, downsample the data to 256 Hz, and remove the linear trend of the data. The data are then converted into the common average montage. We extract 0.5-second time segments around the labeled spikes and normal background activities, where the middle 0.25-second segment is of our interest and the remaining serves as reference signals. Finally, we apply the pre-trained model from the UCSF MEG data on the out-of-sample EEG data, to evaluate NDL’s adaptability across different datasets.

3 Model

Let $\mathbf{X}_i = \{\mathbf{X}_{il}, l = 1, \dots, d\}^\top$ be a random matrix representing a segment of multi-channel signals, where d is the number of channels, \mathbf{X}_{il} is a T -dimensional vector representing the signals in Channel l with T time measurements. We aim to predict whether the segment

\mathbf{X}_i contains a spike or not. Let Y_i be a binary indicator, where $Y_i = 1$ indicates that a spike appears in at least one channel in the segment \mathbf{X}_i , and $Y_i = 0$ indicates that no spike appears in the segment. Furthermore, let $\mathbf{Z}_i = \{\mathbf{Z}_{il}, l = 1, \dots, d\}^\top$ represent a segment of background signals surrounding \mathbf{X}_i , where \mathbf{Z}_{il} is a p -dimensional vector containing signals from p time measurements in Channel l . We assume that $\{Y_i, \mathbf{X}_i, \mathbf{Z}_i\}$, $i = 1, \dots, n$, are independent identically distributed. Figure 2 provides two exemplary segments where $Y_i = 0$ and $Y_j = 1$, with the corresponding $\{\mathbf{X}_i, \mathbf{Z}_i\}$ and $\{\mathbf{X}_j, \mathbf{Z}_j\}$.

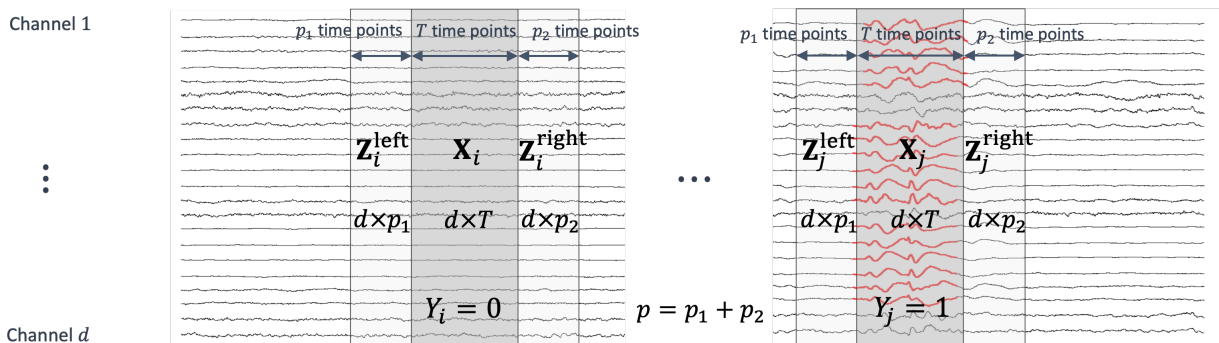


Figure 2: Illustration of $\{Y_i = 0, \mathbf{X}_i, \mathbf{Z}_i\}$ (left) and $\{Y_j = 1, \mathbf{X}_j, \mathbf{Z}_j\}$ (right). Spike signals are annotated in red and bold while background signals are shown in black. In the TUH data of Section 2.1, we set $d = 22$, $T = p = 250$, $p_1 = p_2 = 125$.

We define a channel-specific weight function as $\boldsymbol{\alpha}(\mathbf{X}_{il}, \mathbf{X}_i) = \{\alpha_k(\mathbf{X}_{il}, \mathbf{X}_i), k = 1, \dots, p\}^\top$, where $\alpha_k(\mathbf{X}_{il}, \mathbf{X}_i) = \exp\{\omega_k(\mathbf{X}_{il})\} / \sum_{l=1}^d \exp\{\omega_k(\mathbf{X}_{il})\}$ represents the k -th weight, dynamically standardized across d channels. Here, $\omega_k(\mathbf{X}_{il})$, $k = 1, \dots, p$, are unknown real-valued functions. The weight function $\boldsymbol{\alpha}(\mathbf{X}_{il}, \mathbf{X}_i)$ incorporates information from all channels while placing particular emphasis on Channel l , highlighting the importance of signal patterns in that channel. Then we combine the signals including \mathbf{X}_i and \mathbf{Z}_i , through

$$\mathbf{S}_i(\boldsymbol{\alpha}) \equiv \sum_{l=1}^d \{\mathbf{X}_{il} \boldsymbol{\alpha}(\mathbf{X}_{il}, \mathbf{X}_i)^\top + \mathbf{1}_T \boldsymbol{\alpha}(\mathbf{X}_{il}, \mathbf{X}_i)^\top \mathbf{Z}_{il} \mathbf{1}_p^\top\}, \quad (1)$$

where $\mathbf{1}_T$ and $\mathbf{1}_p$ are T - and p - dimensional one vectors, respectively. We introduce an

unknown real function $g(\cdot) : \mathbb{R}^{T \times p} \rightarrow \mathbb{R}$ to capture the complex relationship between the combination defined in (1) and the response Y_i . We then assume that the conditional probability for $Y_i = 1$ is in the following form:

$$\Pr(Y_i = 1 | \mathbf{X}_i, \mathbf{Z}_i) = \{1 + \exp[-g\{\mathbf{S}_i(\boldsymbol{\alpha})\}]\}^{-1}, \quad (2)$$

where g and $\boldsymbol{\alpha}$ are unknown functions that need to be estimated.

Proposition 1 *Assume $g(\cdot)$ is continuously differentiable, $\boldsymbol{\alpha}(\mathbf{X}_{il}, \mathbf{X}_i) > 0$ entry-wise and $\sum_{l=1}^d \boldsymbol{\alpha}(\mathbf{X}_{il}, \mathbf{X}_i) = \mathbf{1}$. Then $\boldsymbol{\alpha}(\mathbf{X}_{il}, \mathbf{X}_i)$ and $g(\cdot)$ are identifiable.*

Remark 1 *Assuming $\sum_{l=1}^d \boldsymbol{\alpha}(\mathbf{X}_{il}, \mathbf{X}_i) = \mathbf{1}$ is essential for the identifiability of the model. Based on this assumption, we propose the softmax-standardized form of $\boldsymbol{\alpha}$. In the formulation (1), the term $\sum_{l=1}^d \mathbf{X}_{il} \boldsymbol{\alpha}(\mathbf{X}_{il}, \mathbf{X}_i)^\top$ maps the signals \mathbf{X}_i from d channels onto a shared p -dimensional space. Intuitively, a higher value of $\|\boldsymbol{\alpha}(\mathbf{X}_{il}, \mathbf{X}_i)\|_2$ indicates a greater contribution of Channel l to the outcome. It is worth noting that using only this term makes the model unidentifiable because the order of the columns of $\boldsymbol{\alpha}(\mathbf{X}_{il}, \mathbf{X}_i)$ can vary arbitrarily. The term $\sum_{l=1}^d \mathbf{1}_T \boldsymbol{\alpha}(\mathbf{X}_{il}, \mathbf{X}_i)^\top \mathbf{Z}_{il} \mathbf{1}_p^\top$ is introduced to address this problem. By multiplying each element of $\boldsymbol{\alpha}(\mathbf{X}_{il}, \mathbf{X}_i)$ with a distinct element of \mathbf{Z}_{il} , we effectively fix the order of the columns of $\boldsymbol{\alpha}(\mathbf{X}_{il}, \mathbf{X}_i)$, ensuring the identifiability of the model.*

In the model, the dimension p , i.e. the dimension of \mathbf{Z}_{il} and the dimension of $\boldsymbol{\alpha}(\mathbf{X}_{il}, \mathbf{X}_i)$, should be selected appropriately depending on the context. When $p < T$, a low-dimensional embedding of the data is obtained, which can be beneficial for dimension reduction in analyses involving a large number of time points. This approach is particularly useful for tasks such as seizure detection or resting-state signal classification, where signal recordings span across minutes or hours. In contrast, when $p = T$, all the original signal information is preserved. This choice is recommended for tasks like spike detection, where the analysis

involves only short data segments, typically containing less than 100 time points. We set $p = T$ for the real data analyses in this paper. We select symmetric intervals $\mathbf{Z}_i^{\text{left}}$ and $\mathbf{Z}_i^{\text{right}}$ primarily for convenience. Moreover, by definition, a spike must stand out against its surrounding background, so we sample background segments around each identified spike. Since there is no clinical evidence that pre-spike and post-spike backgrounds differ in informational content, we deliberately choose a symmetric background window to avoid introducing any bias.

Our proposal is related to, but distinct from, both the attention mechanism (Vaswani et al. 2017) and the Mixture-of-Experts model (Jacobs et al. 1991). We define a weight function $\alpha(\mathbf{X}_{it}, \mathbf{X}_i)$ to represent channel importance as a function of the signal itself. While this resembles the key-query weighting in attention and the weighted combination in Mixture-of-Experts, our method introduces structural constraints on the weight function, which preserve model identifiability and enhance interpretability.

4 Deep Learning Estimation

Deep neural networks (DNNs) have emerged as powerful tools for estimating unknown functions in the nonparametric regression. Yarotsky (2017) and Imaizumi and Fukumizu (2019) demonstrate that deep neural networks (DNNs) outperform other models in approximating unknown nonparametric functions. Furthermore, Schmidt-Hieber (2020) provides comprehensive analyses showing that deep networks achieve minimax optimal rates for estimating Hölder smooth functions. To flexibly capture the structures of the unknown functions g and α in Model (2), we adopt DNNs with the ReLU activation function (Schmidt-Hieber 2020) to approximate the underlying true functions g^* and α^* .

More specifically, let network architectures with L numbers of layers and a width vector

\mathbf{p}_w , where $\mathbf{p}_w = (p_{w0}, \dots, p_{w(L+1)}) \in \mathbb{N}^{L+1}$, represent any function in the form of

$$f : \mathbb{R}^{p_{w0}} \rightarrow \mathbb{R}^{p_{w(L+1)}}, \mathbf{x} \rightarrow f(\mathbf{x}) \equiv \mathbf{W}_L \sigma_{\mathbf{v}_L} \mathbf{W}_{L-1} \sigma_{\mathbf{v}_{L-1}}, \dots, \mathbf{W}_1 \sigma_{\mathbf{v}_1} \mathbf{W}_0 \mathbf{x}, \quad (3)$$

where $\sigma_{\mathbf{v}}(y_1, \dots, y_r) = \{\sigma(y_1 - v_1), \dots, \sigma(y_r - v_r)\}$ is a vector of ReLU activation functions, \mathbf{W}_i is a $p_{w(i+1)} \times p_{wi}$ weight matrix, and $\mathbf{v}_i \in \mathbb{R}^{p_{wi}}$ is a shift vector. Then we denote the set of these neural network functions with s numbers of nonzero parameters as

$$\mathcal{F}(L, \mathbf{p}_w, s, F) \equiv \left\{ f \text{ of the form (3)} : \max_{j=0, \dots, L} \max(\|\mathbf{W}_j\|_\infty, \|\mathbf{v}_j\|_\infty) \leq 1, \right. \\ \left. \sum_{j=1}^L \|\mathbf{W}_j\|_0 + \|\mathbf{v}_j\|_0 \leq s, \sup_{\mathbf{x}} |f(\mathbf{x})| \leq F \right\}.$$

Denote $\mathcal{F}_f = \mathcal{F}(L_f, \mathbf{p}_f, s_f, F_f)$, where f can be $g, \omega_k, k = 1, \dots, p$.

Furthermore, we define a general form of the true function space as follows.

Definition 1 Define the set of β -Hölder functions with radius K as

$$\mathcal{C}_t^\beta(D, K) \equiv \left\{ f : D \subset \mathbb{R}^t \rightarrow \mathbb{R} : \right. \\ \left. \sum_{\gamma: \|\gamma\|_1 < \beta} \|\partial^\gamma f\|_\infty + \sum_{\gamma: \|\gamma\|_1 = \lfloor \beta \rfloor} \sup_{\mathbf{x}_1, \mathbf{x}_2 \in D, \mathbf{x}_1 \neq \mathbf{x}_2} \frac{|\partial^\gamma f(\mathbf{x}_1) - \partial^\gamma f(\mathbf{x}_2)|}{\|\mathbf{x}_1 - \mathbf{x}_2\|_\infty^{\beta - \lfloor \beta \rfloor}} \leq K \right\},$$

where $\partial^\gamma = \partial^{\gamma_1} \dots \partial^{\gamma_t}$ with $\gamma = (\gamma_1, \dots, \gamma_t)^\top \in \mathbb{N}^t$, and $\lfloor \beta \rfloor$ denotes the largest integer strictly smaller than β . Then the set of true function space is defined as

$$\mathcal{G}(q, \mathbf{d}, \mathbf{t}, \boldsymbol{\beta}, K) \equiv \left\{ f = g_q \circ \dots \circ g_0 : g_u \equiv (g_{uj})_j : [a_u, b_u]^{d_u} \rightarrow [a_{u+1}, b_{u+1}]^{d_{u+1}}, \right. \\ \left. g_{uj} \in \mathcal{C}_{t_u}^{\beta_u}([a_u, b_u]^{t_u}, K), \text{ for some } |a_i|, |b_i| < K \right\},$$

where $\mathbf{d} \equiv (d_0, \dots, d_{q+1})$, $\mathbf{t} \equiv (t_0, \dots, t_q)^\top$ and $\boldsymbol{\beta} \equiv (\beta_0, \dots, \beta_q)^\top$.

For notational convenience, we denote the true function space for an arbitrary function f as $\mathcal{G}_f \equiv \mathcal{G}(q_f, \mathbf{d}_f, \mathbf{t}_f, \boldsymbol{\beta}_f, K_f)$. Assume that $g^* \in \mathcal{G}_g, \omega_k^* \in \mathcal{G}_{\omega_k}$ are the true functions of g, ω_k .

Let $\alpha_k^*(\mathbf{X}_{il}, \mathbf{X}_i) = \exp\{\omega_k^*(\mathbf{X}_{il})\} / \sum_{l=1}^d \exp\{\omega_k^*(\mathbf{X}_{il})\}$ and $\boldsymbol{\alpha}^*(\mathbf{X}_{il}, \mathbf{X}_i) = \{\alpha_k^*(\mathbf{X}_{il}, \mathbf{X}_i), k = 1, \dots, p\}^\top$. We can estimate $g^*, \boldsymbol{\alpha}^*$ by minimizing the negative log-likelihood

$$\begin{aligned} \mathcal{L}(g, \boldsymbol{\alpha}) &= -n^{-1} \sum_{i=1}^n (Y_i g\{\mathbf{S}_i(\boldsymbol{\alpha})\} - h[g\{\mathbf{S}_i(\boldsymbol{\alpha})\}]) \text{ subject to} \\ g &\in \mathcal{F}_g, \omega_k \in \mathcal{F}_{\omega_k}, \alpha_k(\mathbf{X}_{il}, \mathbf{X}_i) = \exp\{\omega_k(\mathbf{X}_{il})\} / \sum_{l=1}^d \exp\{\omega_k(\mathbf{X}_{il})\}, \\ \boldsymbol{\alpha}(\mathbf{X}_{il}, \mathbf{X}_i) &= \{\alpha_k(\mathbf{X}_{il}, \mathbf{X}_i), k = 1, \dots, p\}^\top \end{aligned} \quad (4)$$

where $h(x) = \log\{1 + \exp(x)\}$. Let $\hat{g}, \hat{\boldsymbol{\alpha}}$ be the resulting estimators.

In practice, we employ the network architecture depicted in Figure 3 to approximate the true functions $g^*, \boldsymbol{\alpha}^*$. As shown in Figure 3, the core structure consists of a series of recursive CNN layers followed by a fully connected layer. We use Blocks 1 and 2 to construct functions in \mathcal{F}_{ω_k} , $k = 1, \dots, p$, which approximate $\boldsymbol{\alpha}^*$. The resulting function is then fed into Blocks 3 and 4 to build a function in \mathcal{F}_g that approximates g^* .

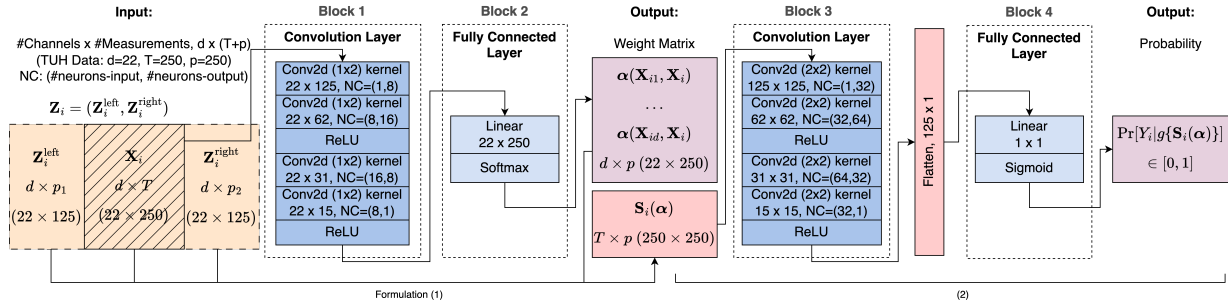


Figure 3: The DNN diagram to approximate the true functions $g^*, \boldsymbol{\alpha}^*$.

We establish the asymptotic consistency of the estimators under the Conditions (C1)–(C6), which are presented in Section S4 in the supplementary material. Here, we first introduce some necessary definitions. Let $g_0 \in \mathcal{F}_g, \omega_{0k} \in \mathcal{F}_{\omega_k}, k = 1, \dots, p$ such that $g_0 \equiv \operatorname{argmin}_{g \in \mathcal{F}_g} \|g - g^*\|_\infty$, and $\omega_{0k} \equiv \operatorname{argmin}_{\omega_k \in \mathcal{F}_{\omega_k}} \|\omega_k - \omega_k^*\|_\infty$, where g^*, ω_k^* are the true functions in $\mathcal{G}_g, \mathcal{G}_{\omega_k}$, respectively. Let $\alpha_{0k}(\mathbf{X}_{il}, \mathbf{X}_i) = \exp\{\omega_{0k}(\mathbf{X}_{il})\} / \sum_{l=1}^d \exp\{\omega_{0k}(\mathbf{X}_{il})\}$ and $\boldsymbol{\alpha}_0 = \{\alpha_{0k}, k = 1, \dots, p\}^\top$. Let $\psi_g = g - g_0$ and $\psi_{\alpha_k} = \alpha_k - \alpha_{0k}$ for arbitrary functions

$g \in \mathcal{F}_g$ and $\alpha_k \in \mathcal{H}_{\alpha_k}$, where

$$\mathcal{H}_k \equiv \left\{ \alpha_k = \exp\{\omega_k(\mathbf{X}_{il})\} / \sum_{l=1}^d \exp\{\omega_k(\mathbf{X}_{il})\} : \omega_k \in \mathcal{F}_{\omega_k}, k = 1, \dots, p \right\}.$$

Lemma 1 *Assuming Conditions (C1)–(C5) in the supplementary material hold, and $T, p \leq s_g$, there are positive constants $C_g, C_{\omega_j}, c_g, c_{\omega_j}$ such that, with probability one,*

$$\begin{aligned} |h'[g^* \{\mathbf{S}_i(\boldsymbol{\alpha}^*)\}] - h'[g_0 \{\mathbf{S}_i(\boldsymbol{\alpha}_0)\}]| \leq & \left\{ C_g \max_{u=0, \dots, q_g} c_g^{-\frac{\beta_{gu}^*}{t_{gu}}} n^{-\frac{\beta_{gu}^*}{2\beta_{gu}^* + t_{gu}}} \right. \\ & \left. + 2C_M M_L \sqrt{d \min(s_g, Tp)} \sup_{j=1, \dots, p} C_{\omega_j} \max_{u=0, \dots, q_{\omega_j}} c_{\omega_j}^{-\frac{\beta_{\omega_j u}^*}{t_{\omega_j u}}} n^{-\frac{\beta_{\omega_j u}^*}{2\beta_{\omega_j u}^* + t_{\omega_j u}}} \right\}. \end{aligned}$$

The proof of Lemma 1 is presented in Section S5 in the supplementary material. Note that $h'(\cdot)$ is the expit function: $h'[g^* \{\mathbf{S}_i(\boldsymbol{\alpha}^*)\}]$ represents the true probability of $Y_i = 1$. Lemma 1 shows that the distance between the deep learning approximation of the success probability and the truth depends on how well g_0 and $\boldsymbol{\alpha}_0$ approximate the true values. This distance decreases at the standard nonparametric rate as the sample size grows.

Theorem 1 *Let $\psi_{\hat{g}} = \hat{g} - g_0$ and $\psi_{\hat{\alpha}_j} = \hat{\alpha}_j - \alpha_{0j}$. Assume $\hat{\alpha}_j, \alpha_{0j} \in \mathcal{H}_j$, $\omega_j^* \in \mathcal{G}_{\omega_j}$, $\hat{g}, g_0 \in \mathcal{F}_g$, and $g^* \in \mathcal{G}_g$. Assume $T, p < s_g$ and Conditions (C1)–(C6) in the supplementary material hold. Let $dP_{\boldsymbol{\alpha}}(\cdot)$ be the probability density function of $\mathbf{S}_i(\boldsymbol{\alpha})$, and assume $\|dP_{\boldsymbol{\alpha}_0}(\mathbf{z})/dP_{\boldsymbol{\alpha}^*}(\mathbf{z})\|_{\infty} \geq m_h > 0$. Furthermore, let $dP_{\mathbf{X}}(\cdot)$ be the probability density for \mathbf{X}_i . When $n \rightarrow \infty$ and T, p are finite, we have*

$$\int \{\hat{g}(\mathbf{z}) - g^*(\mathbf{z})\}^2 dP_{\boldsymbol{\alpha}^*}(\mathbf{z}) + \sum_{j=1}^p \int \sum_{l=1}^d \{\hat{\alpha}_j(\mathbf{x}_l, \mathbf{x}) - \alpha_{0j}^*(\mathbf{x}_l, \mathbf{x})\}^2 dP_{\mathbf{X}}(\mathbf{x}) \xrightarrow{p} 0.$$

A more comprehensive version of the theorem, including its convergence rate, is presented as Theorem S1 in Section S7 of the supplementary material. The proof of the main theorem is provided in Section S8. To establish the result, we first show in Lemma S6 that the first derivative of the objective function is upper bounded by a term that vanishes as the sample

size increases. Next, Lemma S7 demonstrates that the second derivative converges to a positive definite matrix. Building on these, we prove estimation consistency by combining the first- and second-order rates in Lemma 1. Additionally, Section S9 in the supplementary material provides examples that illustrate special cases of compositional constraints on ω_k for $k = 1, \dots, p$, and on g . Section S10 provides the convergence on the simulated data.

5 Real Data Analysis

We apply NDL on the three real datasets described in Section 2, including the TUH dataset, the UCSF MEG dataset and the BTH EEG dataset. We also compare NDL with three existing methods: SpikeDet, which uses template matching (Nonclercq and Ercek 2016); a deep learning multi-head CNN model trained on the TUH dataset (Munia et al. 2023); and SpikeNet, a deep learning approach developed using a private dataset of 9,571 scalp EEG recordings from Massachusetts General Hospital (Jing et al. 2020).

5.1 Results from the TUH Data

We apply NDL to classify the EEG segments from the TUH data into normal and abnormal waveforms. In the testing set, the i th segment is classified as containing an abnormal waveform if the predicted probability of $Y_i = 1$ is greater than 0.5. We report the following evaluation metrics, where TP , TN , FP , and FN denote true positives, true negatives, false positives and false negatives, respectively.

1. Sensitivity $:= TP/(TP + FN)$
2. Precision $:= TP/(TP + FP)$
3. Specificity $:= TN/(TN + FP)$

4. F1 score := $TP / (TP + (FP + FN) / 2)$
5. PRAUC: The area under the precision-recall curve
6. AUC: The area under the receiver operating characteristic (ROC) curve.

The TUH dataset is divided into 80% for training and 20% for testing. We use the mini-batch gradient descent to train the loss function. The learning rate is stepwise and decays by 0.5 every 10 epochs. The training loss decreases rapidly in the first 10 epochs and becomes stable after the 40th epoch.

Figures 4 (a) and (b) show the ROC curve and precision-recall curve on the test set. The AUC and PRAUC are 93.35% and 92.14%, respectively, demonstrating the high accuracy and precision of the proposed method. Table 2 compares NDL with three competing methods: SpikeDet (Nonclercq and Ercek 2016), an open-source spike detection algorithm developed by Nonclercq et al. (2009); a deep multi-head CNN model proposed in Munia et al. (2023); and SpikeNet developed by Jing et al. (2020). It is worth noting that SpikeNet is a large-scale deep learning model, comprising 318,849 parameters and trained on EEG data from over 19 million EEG segments. As such, it is regarded as the current state-of-the-art benchmark method.

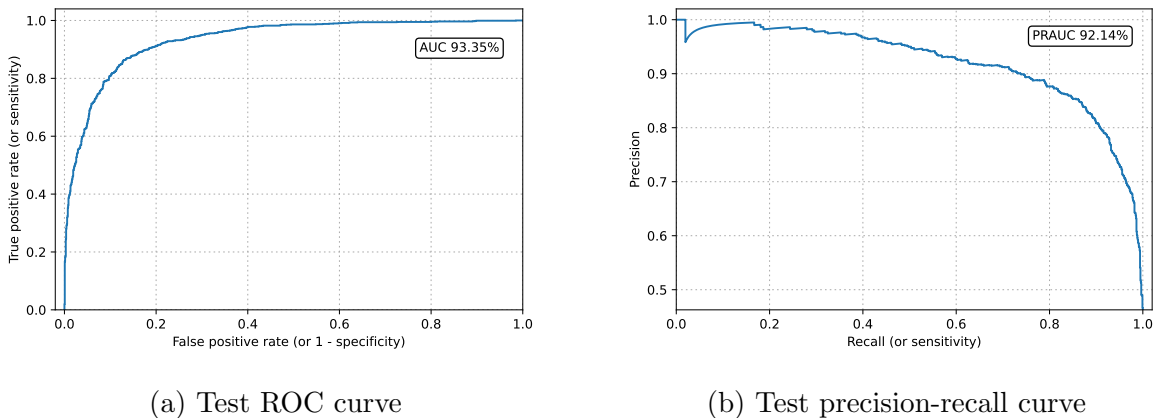


Figure 4: TUH: Test results from NDL with fine-tuned hyperparameters.

Table 2: TUH: Comparison of NDL, SpikeNet, Multi-head CNN, and SpikeDet. Specificity, PRAUC and AUC are not reported for Multi-head CNN. PRAUC and AUC are unavailable in SpikeDet, which generates binary outputs rather than probabilities.

TUH Data	Sen (%)	Prec (%)	Spec (%)	F1 (%)	PRAUC (%)	AUC (%)
NDL	86.96	84.51	86.27	85.71	92.14	93.35
SpikeNet	81.33	86.96	89.50	84.05	90.02	89.63
Multi-head CNN	74.71	72.70	-	73.69	-	-
SpikeDet	13.30	78.39	96.84	22.74	-	-

Table 2 demonstrates that NDL achieves the best performance among all methods, with the highest sensitivity, F1 score, PRAUC, and AUC (highlighted in bold). In this comparison, NDL, SpikeNet and Multi-head CNN method are deep learning-based methods. NDL and Multi-head CNN are trained and evaluated on the TUH dataset, whereas SpikeNet is pre-trained on one of the largest private EEG datasets (Jing et al. 2020) and then tested on the TUH test set. In contrast, SpikeDet is an unsupervised template matching method, which does not consider spike patterns from noisy data. Therefore, SpikeDet gives the highest number of false negatives among the four methods.

In addition to binary classification, NDL can identify the channel from which the spike likely originates. Specifically, for each channel l , NDL estimates a p -dimensional weight vector $\hat{\alpha}(\mathbf{X}_{il}, \mathbf{X}_i)$. By summing its entries, we obtain an importance score for Channel l as $\mathbf{1}^\top \hat{\alpha}(\mathbf{X}_{il}, \mathbf{X}_i)$. Ranking these scores across all channels allows us to identify the top L channels most likely to contain spikes.

To assess this approach, we cross-check the selected top channels with the actual channel labels from the TUH data to check whether our model can identify spike-containing channels

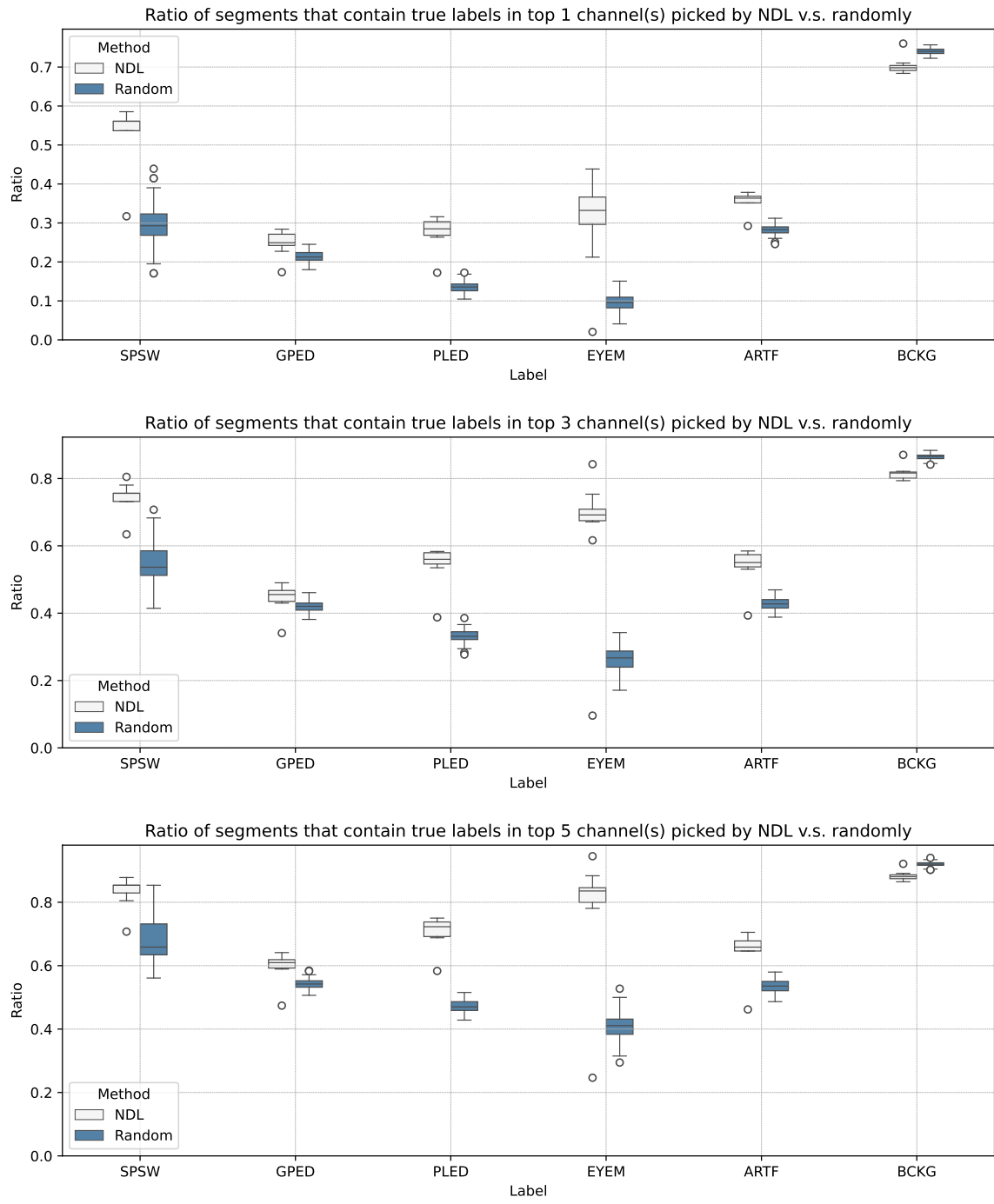


Figure 5: TUH: Side-by-side boxplots comparing the top channels selected by NDL ranking with random ranking through 100 repetitions.

better than random selection. Figure 5 illustrates the probability that the top L channels of a segment contain a true spike, comparing NDL ranking with random ranking based on the TUH testing data. We create the 95% confidence interval of the probability through resampling procedures with different initial values generated from different random seeds. It is obvious that NDL performs much better in identifying those channels with spikes. Furthermore, NDL ignores background channels (last pair of side-by-side boxplots).

5.2 Results from the UCSF MEG Data

We use 95% of the data for training and the remaining 5% for testing. Table 3 summarizes NDL’s excellent performance on the testing data, for example, an AUC of 91.61%.

Table 3: UCSF MEG: Testing Results.

UCSF MEG Data	Sen (%)	Prec (%)	Spec (%)	F1 (%)	PRAUC (%)	AUC (%)
NDL	77.07	84.26	91.39	80.50	87.20	91.61

We visualize the distribution of the most important channels using topographical graphs (Figure 6) and barplots (Figure 7), where the topographical graph is a 2D representation of the probabilities of being the top L channels identified by NDL ranking.

Figure 6 contains six topographical graphs, illustrating the probabilities of being identified as one of the most important L channels out of the 140 MEG channels based on the training set and the testing set, respectively. Figure 7 shows the distribution of the top L channels across different brain lobes. Figures 6 and 7 both indicate that the spikes often occur in the temporal lobes. This is consistent with the clinical finding that seizures usually happen in the temporal lobes (McIntosh and Das 2019).

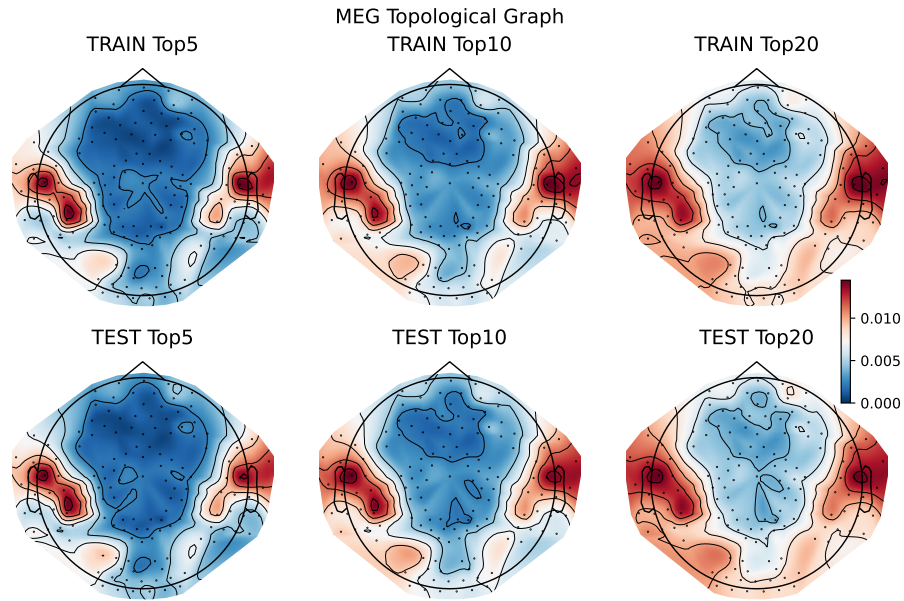


Figure 6: UCSF MEG: The topological distributions of the probabilities of being the top channels identified by NDL ranking.

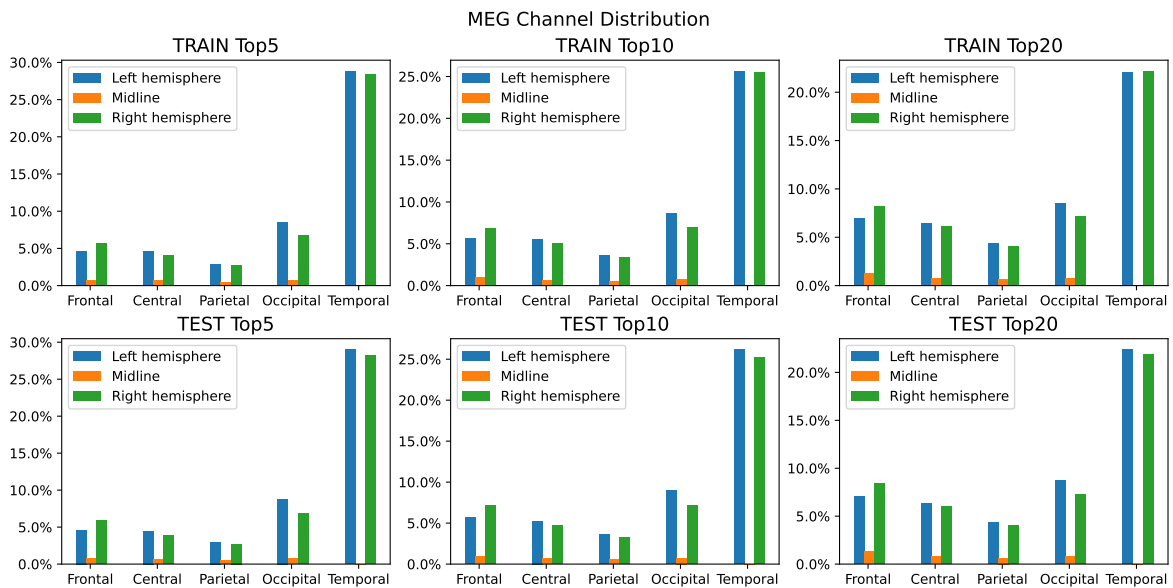


Figure 7: UCSF MEG: Histograms of the distributions of the top channels identified by NDL ranking, on five different lobes.

5.3 Results from the BTH EEG Data

We take the model trained on the UCSF MEG dataset and test it on the BTH EEG dataset. This analysis aims to evaluate the adaptability of NDL across different modalities with varying channels.

We evaluate the performance of NDL on 50 randomly selected subsets of the BTH EEG dataset (Section 2.3) and compare it against SpikeNet, the strongest competing method. NDL achieves an AUC ranging from 79.60% to 90.00%, a PRAUC from 77.04% to 91.41%. In comparison, SpikeNet achieves an AUC between 84.23% and 93.52%, a PRAUC between 79.39% and 95.24%. Despite being trained on only 230,325 MEG segments and using just 17,683 parameters, NDL achieves performance comparable to the much larger SpikeNet model, which was trained on over 19 million EEG segments and contains more than 300,000 parameters. Furthermore, these results demonstrate that NDL generalizes well to out-of-sample, cross-modality settings.

A key advantage of NDL over SpikeNet is its flexibility in handling channel variabilities—NDL remains effective even when certain channels fail to capture brain signals or when additional channels are introduced to improve spatial resolution. In contrast, SpikeNet becomes unusable when the channel configuration deviates from that of the training data, as it was trained under fixed channel settings.

We present three topographical graphs in Figure 8 showing the probability of each channel being selected as one of the top L channels by NDL. Furthermore, Figure 9 shows the distribution of the top L channels in different lobes. Interestingly, in addition to the temporal lobes, the prefrontal regions are often selected. Our neurology collaborators confirm that this is not unexpected, as scalp EEG spikes can often be confused with eye movements, which typically occur in the prefrontal areas. More data are needed to fine-tune

the model for better adaptation to the EEG data.

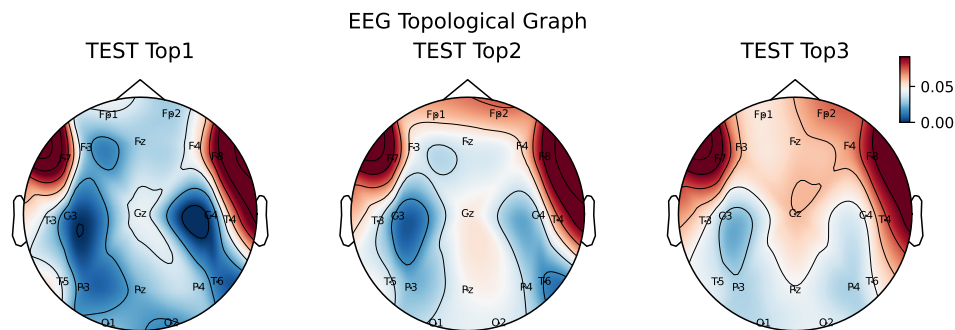


Figure 8: BTH EEG: The topological distributions of the probabilities of being selected into the top channels NDL ranking.

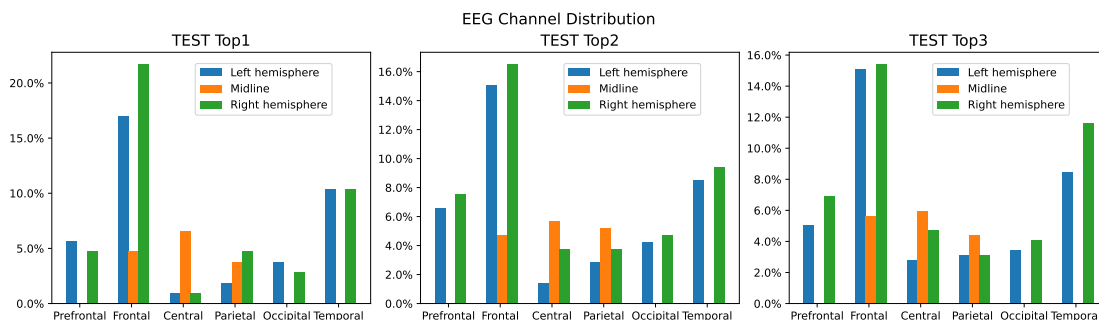


Figure 9: BTH EEG: Histograms of the distributions of the top channels selected by NDL ranking, on six different lobes.

5.4 Procedures to adopt to continuous time series data

Unlike the segmented data analyzed in the previous subsections, neurophysiology data are usually recorded continuously in real-world settings. We develop the following Algorithm 1 that applies NDL to continuous time series data in practice.

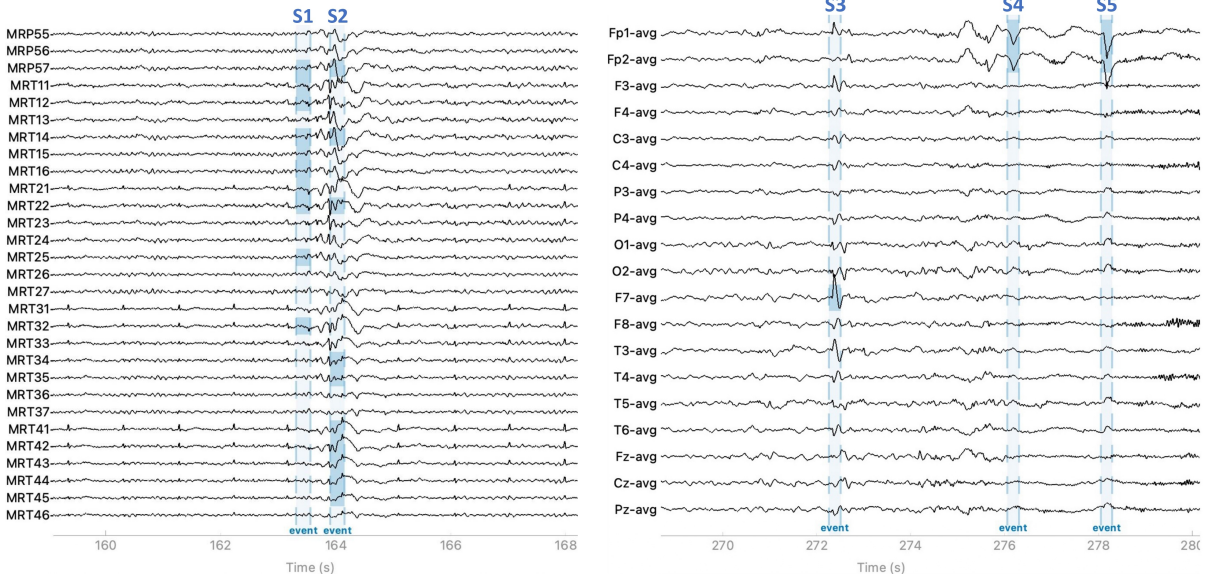
Algorithm 1 employs a sliding window technique to extract overlapping data segments and evaluate the probability of containing a spike for each segment. We then identify those time segments where the probability exceeds a specified threshold C as initial candi-

dates. Finally, we apply a non-maximum suppression algorithm to eliminate overlapping candidates, resulting in the final set of confirmed segments.

Algorithm 1 The sliding window algorithm

- Input:** Preprocessed MEG and EEG recordings with d channels and a total of T_0 time measurements; a segmentation time length T ; a cutoff C .
- 1: **for** $t = T/2, \dots, T_0 - T/2$ **do**
 - 2: Set the window between the $(t - T/2 + 1)$ th and the $(t + T/2)$ th time points.
 - 3: Estimate the probability $\hat{g}_{(t)}$ and the weight $\hat{\alpha}_{(l,t)}$ for Channel l .
 - 4: **if** $\hat{g}_{(t)} > C$ and $\mathbf{1}^\top \hat{\alpha}_{(l,t)} > (1.5/d)(\sum_{l=1}^d \mathbf{1}^\top \hat{\alpha}_{(l,t)})$ **then**
 - 5: Select the segment between the window as a candidate.
 - 6: **end if**
 - 7: Remove duplicates by clustering the candidate segments based on time, utilizing the Density-Based Spatial Clustering of Applications with Noise (DBSCAN) method (Ester et al. 1996).
 - 8: Select the segment with the highest spike probability within each cluster as the final representation.
 - 9: **end for**
-

We apply Algorithm 1 to the testing set of the UCSF MEG data and to the BTH EEG Data. Figure 10(a) presents the results of applying NDL to a continuous MEG recording from UCSF. The detection S1 accurately identifies the true spikes in the right temporal lobe, followed by an additional detection S2 shortly afterward. Although S2 appears outside the 0.25-second window according to the true spike labels, the detection remains valid since the true labels mark the onset of the spikes, and spikes may propagate to other channels over time. Moreover, our detection effectively highlights the channels where spikes occur, showing its accuracy in identifying spike-related activity across multiple channels.



(a) MEG

(b) EEG

Figure 10: MEG and EEG recordings annotated by NDL using Algorithm 1, with top channels highlighted in a dark color for each detection.

Figure 10(b) shows the results of applying NDL to the continuous EEG data from BTH. The detection S3 accurately identifies a true spike on the F7-avg channel. The detections S4 and S5 capture eye movements on the Fp1-avg and Fp2-avg channels, respectively. Eye movement artifacts typically appear simultaneously on these two channels since they are closest to the eyes. In practice, if both channels are identified as important, it is likely that the detection relates to eye movements rather than true spikes. Identification of key channels plays a crucial role in reducing false positives by helping to distinguish between eye movement artifacts and genuine spike activities.

6 Conclusion and Discussion

We have developed the NDL method as an interpretable alternative to traditional deep learning methods for spike detection. This method can adapt to different channel types,

making it a foundational model for neurophysiological data analysis. We have established the model’s identifiability and demonstrated the asymptotic consistency of its estimation procedure. NDL has been applied to the publicly available TUH data, the private UCSF MEG data, and the private BTH EEG data. Our analyses show that NDL outperforms existing methods in terms of sensitivity and specificity in spike detection. Moreover, it effectively identifies channels containing relevant events. Finally, we demonstrate that a model trained on the UCSF MEG data can be successfully applied to the BTH EEG data, highlighting NDL’s capacity to integrate multiple datasets and serve as a foundation model that can be fine-tuned for different targets.

In this paper, our model is trained on the TUH data from 370 subjects and the UCSF MEG data from 277 subjects. Due to the limited sample sizes, the model may not fully capture the variation in spike waveforms across different populations. We are currently collaborating with clinicians to label more EEG and MEG data to improve the model’s accuracy across a broader range of populations. The tools developed in this paper will be used as a screening process to identify spike candidates, streamlining the labeling process in this larger study.

False discovery has long been a challenge in spike detection, and we acknowledge that our model trained on the limited samples does not fully address this issue. However, identifying key relevant channels can help reduce false discoveries. For instance, if the first two detected channels are those nearest to the eyes, the spike is more likely related to eye movements. Additionally, training the model on larger datasets, which we are currently preparing, could significantly lower the false discovery rate.

Data Availability Statement

The TUH data that support the findings of this study are available from the TUH EEG Corpus. Restrictions apply to the availability of these data, which were used under license for this study. Data are available at <https://www.isip.piconepress.com/projects/nedc/data/> with the permission of The Neural Engineering Data Consortium.

Due to the nature of the research, the UCSF MEG data and the BTH EEG data are not available due to commercial restrictions.

Acknowledgement

The computations were performed using research computing facilities offered by Information Technology Services, the University of Hong Kong and by the Department of Radiology, the University of California, San Francisco.

Funding

The work of Wei and Shen is partially supported by a HKSAR UGC CRF grant (C7162-20G). The work of Fei Jiang is supported by NIH grants K25AG071840 and R01NS132766.

References

Antoniades, A., Spyrou, L., Took, C. C., and Sanei, S. (2016), “Deep learning for epileptic intracranial eeg data”, in *2016 IEEE 26th International Workshop on Machine Learning for Signal Processing (MLSP)*, pp. 1–6, DOI: 10.1109/MLSP.2016.7738824.

- Baud, M. O., Kleen, J. K., Anumanchipalli, G. K., Hamilton, L. S., Tan, Y.-L., Knowlton, R., et al. (2018), “Unsupervised learning of spatiotemporal interictal discharges in focal epilepsy”, *Neurosurgery*, 83(4), 683–691, DOI: 10.1093/neuros/nyx480.
- Chung, Y. G., Lee, W.-J., Na, S. M., Kim, H., Hwang, H., Yun, C.-H., et al. (2023), “Deep learning-based automated detection and multiclass classification of focal interictal epileptiform discharges in scalp electroencephalograms”, *Scientific Reports*, 13(1), 6755, DOI: 10.1038/s41598-023-33906-5.
- Clarke, S., Karoly, P. J., Nurse, E., Seneviratne, U., Taylor, J., Knight-Sadler, R., et al. (2021), “Computer-assisted eeg diagnostic review for idiopathic generalized epilepsy”, *Epilepsy & Behavior*, 121, 106556, DOI: 10.1016/j.yebeh.2019.106556.
- Ester, M., Kriegel, H.-P., Sander, J., and Xu, X. (1996), “A density-based algorithm for discovering clusters in large spatial databases with noise”, in *Proceedings of the Second International Conference on Knowledge Discovery and Data Mining*, KDD’96, AAAI Press, pp. 226–231, DOI: 10.5555/3001460.3001507.
- Goelz, H., Jones, R. D., and Bones, P. J. (2000), “Wavelet analysis of transient biomedical signals and its application to detection of epileptiform activity in the eeg”, *Clinical electroencephalography*, 31(4), 181–191, DOI: 10.1177/155005940003100406.
- Golmohammadi, M., Harati Nejad Torbati, A. H., Lopez de Diego, S., Obeid, I., and Picone, J. (2019), “Automatic analysis of eegs using big data and hybrid deep learning architectures”, *Frontiers in human neuroscience*, 13, 76, DOI: 10.3389/fnhum.2019.00076.
- Harati, A., Golmohammadi, M., Lopez, S., Obeid, I., and Picone, J. (2015), “Improved eeg event classification using differential energy”, in *2015 IEEE Signal Processing in Medicine and Biology Symposium (SPMB)*, IEEE, pp. 1–4, DOI: 10.1109/SPMB.2015.7405421.

- Imaizumi, M., and Fukumizu, K. (2019), “Deep neural networks learn non-smooth functions effectively”, in *The 22nd international conference on artificial intelligence and statistics*, PMLR, pp. 869–878. Available at <https://proceedings.mlr.press/v89/imaizumi19a.html>.
- Indiradevi, K., Elias, E., Sathidevi, P., Nayak, S. D., and Radhakrishnan, K. (2008), “A multi-level wavelet approach for automatic detection of epileptic spikes in the electroencephalogram”, *Computers in biology and medicine*, 38(7), 805–816, DOI: 10.1016/j.compbiomed.2008.04.010.
- Jacobs, R. A., Jordan, M. I., Nowlan, S. J., and Hinton, G. E. (1991), “Adaptive mixtures of local experts”, *Neural computation*, 3(1), 79–87, DOI: 10.1162/neco.1991.3.1.79.
- Jing, J., Sun, H., Kim, J. A., Herlopian, A., Karakis, I., Ng, M., et al. (2020), “Development of expert-level automated detection of epileptiform discharges during electroencephalogram interpretation”, *JAMA Neurology*, 77(1), 103–108, DOI: 10.1001/jamaneurol.2019.3485.
- Johansen, A. R., Jin, J., Maszczyk, T., Dauwels, J., Cash, S. S., and Westover, M. B. (2016), “Epileptiform spike detection via convolutional neural networks”, in *2016 IEEE International Conference on Acoustics, Speech and Signal Processing (ICASSP)*, IEEE, pp. 754–758, DOI: 10.1109/ICASSP.2016.7471776.
- Lodder, S. S., Askamp, J., and van Putten, M. J. (2013), “Inter-ictal spike detection using a database of smart templates”, *Clinical neurophysiology*, 124(12), 2328–2335, DOI: 10.1016/j.clinph.2013.05.019.
- Lopez, S., Gross, A., Yang, S., Golmohammadi, M., Obeid, I., and Picone, J. (2016), “An analysis of two common reference points for eegs”, in *2016 IEEE sig-*

- nal processing in medicine and biology symposium (SPMB)*, IEEE, pp. 1–5, DOI: 10.1109/SPMB.2016.7846854.
- McIntosh, W. C., and Das, J. M. (2019), *Temporal Seizure*, StatPearls. Available at <https://www.ncbi.nlm.nih.gov/books/NBK549852/>.
- Medvedev, A., Agoureeva, G., and Murro, A. (2019), “A long short-term memory neural network for the detection of epileptiform spikes and high frequency oscillations”, *Scientific reports*, 9(1), 19374, DOI: 10.1038/s41598-019-55861-w.
- Munia, M. S., Nourani, M., Harvey, J., and Dave, H. (2023), “Interictal epileptiform discharge detection using multi-head deep convolutional neural network”, in *2023 45th Annual International Conference of the IEEE Engineering in Medicine & Biology Society (EMBC)*, IEEE, pp. 1–4, DOI: 10.1109/EMBC40787.2023.10340735.
- Nonclercq, A., and Ercek, R. (2016), “Spikedet: a spm eeg spike detection toolbox”. Available at <http://beams.ulb.ac.be/research-projects/spm-eeg-spike-detection-toolbox>.
- Nonclercq, A., Foulon, M., Verheulpen, D., De Cock, C., Buzatu, M., Mathys, P., et al. (2009), “Spike detection algorithm automatically adapted to individual patients applied to spike and wave percentage quantification”, *Neurophysiologie Clinique/Clinical Neurophysiology*, 39(2), 123–131, DOI: 10.1016/j.neucli.2008.12.001.
- Obeid, I., and Picone, J. (2016), “The temple university hospital eeg data corpus”, *Frontiers in neuroscience*, 10, 195498, DOI: 10.3389/fnins.2016.00196.
- Schmidt-Hieber, J. (2020), “Nonparametric regression using deep neural networks with ReLU activation function”, *The Annals of Statistics*, 48(4), 1875 – 1897, DOI: 10.1214/19-AOS1875.

- Smith, E. H., Liou, J.-y., Merricks, E. M., Davis, T., Thomson, K., Greger, B., et al. (2022), “Human interictal epileptiform discharges are bidirectional traveling waves echoing ictal discharges”, *Elife*, 11, e73541, DOI: 10.7554/eLife.73541.
- Thomas, J., Jin, J., Thangavel, P., Bagheri, E., Yuvaraj, R., Dauwels, J., et al. (2020), “Automated detection of interictal epileptiform discharges from scalp electroencephalograms by convolutional neural networks”, *International journal of neural systems*, 30(11), 2050030, DOI: 10.1142/S0129065720500306.
- Tjepkema-Cloostermans, M. C., de Carvalho, R. C., and van Putten, M. J. (2018), “Deep learning for detection of focal epileptiform discharges from scalp eeg recordings”, *Clinical neurophysiology*, 129(10), 2191–2196, DOI: 10.1016/j.clinph.2018.06.024.
- Torres, R. E., and Butter, I. H. (1996), “The impact of eeg technology on health manpower”, *American Journal of Electroneurodiagnostic Technology*, 36(2), 114–132, DOI: 10.1080/1086508X.1996.11080544.
- Vaswani, A., Shazeer, N., Parmar, N., Uszkoreit, J., Jones, L., Gomez, A. N., et al. (2017), “Attention is all you need”, *Advances in neural information processing systems*, 30.
- Vershynin, R. (2010), “Introduction to the non-asymptotic analysis of random matrices”, arXiv:1011.3027.
- Wilson, S. B., Turner, C. A., Emerson, R. G., and Scheuer, M. L. (1999), “Spike detection ii: automatic, perception-based detection and clustering”, *Clinical neurophysiology*, 110(3), 404–411, DOI: 10.1016/s1388-2457(98)00023-6.
- World Health Organization (2024), “Epilepsy”. Accessed: 2024-02-07. Available at <https://www.who.int/news-room/fact-sheets/detail/epilepsy>.

Yarotsky, D. (2017), “Error bounds for approximations with deep relu networks”, *Neural Networks*, 94, 103–114, DOI: 10.1016/j.neunet.2017.07.002.

Supplementary Materials for “Nested Deep Learning Model Towards a Foundation Model for Brain Signal Data.”

Fangyi Wei, Jiajie Mo, Kai Zhang, Haipeng Shen,
Srikantan Nagarajan, and Fei Jiang

S1 Additional Notations

We write $a \lesssim b$ if there exists a constant C such that $a \leq Cb$ for all n . Moreover, $a \asymp b$ means that $a \lesssim b$ and $b \lesssim a$. Let $\mathcal{N}(\delta, \mathcal{F}, \|\cdot\|_\infty)$ be the covering number, that is, the minimal number of $\|\cdot\|_\infty$ -balls with radius δ that covers \mathcal{F} . For a variable X , we define $\|X\|_{\psi_2} = \sup_{k \geq 1} k^{-1/2}(E|X|^k)^{1/k}$ and define $\|X\|_{\psi_1} = \sup_{k \geq 1} k^{-1}(E|X|^k)^{1/k}$.

S2 Useful Lemmas

Lemma S1 *Let \mathcal{F} be a sub-field of the sigma-field generated by X . Let $K_j(\mathcal{F}) > 0, j = 1, \dots, 4$ be functions of random variables in \mathcal{F} . Then, the following properties 1, 2, and 3 are equivalent, and when $E(X|\mathcal{F}) = 0$, they are further equivalent to property 4. In addition, $K_j(\mathcal{F})$ can be chosen to satisfy $0 < c < K_j(\mathcal{F})/K_k(\mathcal{F}) < C < \infty$, for all $k, j \in \{1, 2, 3, 4\}$, where c, C are absolute constants.*

1. *Tail: There exists $K_1(\mathcal{F})$ such that $\Pr(|X| > t|\mathcal{F}) \leq \exp\{1 - t^2/K_1^2(\mathcal{F})\}$;*
2. *Moments: There exists $K_2(\mathcal{F})$ such that $E(|X|^k|\mathcal{F})^{1/k} \leq K_2(\mathcal{F})\sqrt{k}$, for all $k \geq 1$;*
3. *Super-exponential moment: There exists $K_3(\mathcal{F})$ such that $E[\exp\{X^2/K_3^2(\mathcal{F})\}|\mathcal{F}] \leq e$;*
4. *Let $E(X|\mathcal{F}) = 0$. There exists $K_4(\mathcal{F})$ such that $E\{\exp(tX)|\mathcal{F}\} \leq \exp\{t^2 K_4^2(\mathcal{F})\}$.*

Definition 2 A random variable X that satisfies one of the equivalent properties in Lemma S1 is named a conditional sub-Gaussian random variable with respect to the sub-sigma field \mathcal{F} . The conditional sub-gaussian norm of X with respect to \mathcal{F} , denoted by $\|X\|_{\psi_2(\mathcal{F})}$, is defined as the smallest $K_2(\mathcal{F})$ in property 2. That is,

$$\|X\|_{\psi_2(\mathcal{F})} = \sup_{k \geq 1} k^{-1/2} E(|X|^k | \mathcal{F})^{1/k}.$$

Lemma S2 Assume $f \in \mathcal{G}(q, \mathbf{d}, \mathbf{t}, \boldsymbol{\beta}, K)$. Furthermore, let $\beta_i^* \equiv \beta_i \prod_{l=i+1}^q \{\min(\beta_l, 1)\}$ and $\phi_n \equiv \max_{i=0, \dots, q} n^{-2\beta_i^*/(2\beta_i^*+t_i)}$. Define a function space $\mathcal{F}(L, (p_{wu})_{u=0, \dots, L+1}, s, F)$ satisfying the following conditions:

- (i) $F \geq \max(K, 1)$,
- (ii) $\sum_{i=0}^q \log_2 \{\max(4t_i, 4\beta_i)\} \log_2 n \leq L \lesssim n\phi_n$,
- (iii) $n\phi_n \lesssim \min_{u=1, \dots, L} p_{wu}$,
- (iv) $s \asymp n\phi_n \log n$.

Then there exists a $f_0 \in \mathcal{F}(L, (p_{wu})_{u=0, \dots, L+1}, s, F)$ such that

$$\|f_0 - f\|_{\infty}^2 \leq C \max_{v=0, \dots, q} c^{-\frac{2\beta_v^*}{t_v}} n^{-\frac{2\beta_v^*}{2\beta_v^*+t_v}}.$$

where C, c are constants only depends on $q, \mathbf{d}, \mathbf{t}, \boldsymbol{\beta}$.

Proof: This lemma is a direct consequence of (26) in Schmidt-Hieber (2020).

Lemma S3 For any $\delta > 0$, we have

$$\log \mathcal{N} \{ \delta, \mathcal{F}(L, \mathbf{p}_w, s, \infty), \|\cdot\|_{\infty} \} \leq (s+1) \log \left\{ 2^{2L+5} \delta^{-1} (L+1) p_{w0}^2 p_{wL+1}^2 s^{2L} \right\}.$$

Proof: This lemma is a direct consequence of Lemma 4 in Schmidt-Hieber (2020).

Lemma S4 Let X_1, \dots, X_N be independent centered sub-Gaussian random variable, and let $K = \max_i \|X_i\|_{\psi_2}$. Then for every $\mathbf{a} = (a_1, \dots, a_N)^\top \in \mathbb{R}^N$ and every $t \geq 0$, we have

$$\Pr \left(\left| \sum_{i=1}^N a_i X_i \right| \right) \leq e \cdot \exp \left(-\frac{ct^2}{K^2 \|\mathbf{a}\|_2^2} \right),$$

where $c > 0$ is an absolute constant.

Proof: This is a direct consequence of Proposition 5.10 in Vershynin (2010).

Lemma S5 Let X_1, \dots, X_N be independent centered sub-exponential random variables, and $K = \max_i \|X_i\|_{\psi_1}$. Then for every $\mathbf{a} = (a_1, \dots, a_N)^\top \in \mathbb{R}^N$ and every $t > 0$, we have

$$\Pr \left(\left| \sum_{i=1}^N a_i X_i \right| \right) \leq 2 \exp \left\{ -c \min \left(\frac{t^2}{K^2 \|\mathbf{a}\|_2^2}, \frac{t}{K \|\mathbf{a}\|_\infty} \right) \right\},$$

where $c > 0$ is an absolute constant.

S3 Proof of Proposition 1

Proof: For notation simplicity, we omit index i in the following proofs. If $\boldsymbol{\alpha}(\mathbf{X}_l, \mathbf{X})$ and the conditional density function $g\{\mathbf{S}(\boldsymbol{\alpha})\}$ are not identifiable, then we will have \tilde{g} , $\tilde{\boldsymbol{\alpha}}$ such that $(g, \boldsymbol{\alpha}) \neq (\tilde{g}, \tilde{\boldsymbol{\alpha}})$, but

$$\begin{aligned} & g \left\{ \sum_{l=1}^d \mathbf{X}_l \boldsymbol{\alpha}(\mathbf{X}_l, \mathbf{X})^\top + \mathbf{1}_T \boldsymbol{\alpha}(\mathbf{X}_l, \mathbf{X})^\top \mathbf{Z}_l \mathbf{1}_p^\top \right\} \\ &= \tilde{g} \left\{ \sum_{l=1}^d \mathbf{X}_l \tilde{\boldsymbol{\alpha}}(\mathbf{X}_l, \mathbf{X})^\top + \mathbf{1}_T \tilde{\boldsymbol{\alpha}}(\mathbf{X}_l, \mathbf{X})^\top \mathbf{Z}_l \mathbf{1}_p^\top \right\} \end{aligned} \quad (\text{S1})$$

for any given $\mathbf{X}_l, \mathbf{Z}_l$. Now replacing \mathbf{Z}_l by $\mathbf{Z}_l + \xi I(\mathbf{X}_l = \mathbf{X}_u) \mathbf{e}_j$ in (S1) where \mathbf{e}_j is a length p unit vector with the j th element 1, and $I(\cdot)$ is an indicator function, Taking the derivative of both sides with respect to ξ and evaluate at $\xi = 0$, denote \mathbf{M}_{qt} be the (q, t) -th entry of matrix, \mathbf{M} , then the left-hand side follows

$$\begin{aligned} & \frac{\partial f \left\{ \sum_{l=1}^d \mathbf{X}_l \boldsymbol{\alpha}(\mathbf{X}_l, \mathbf{X})^\top + \mathbf{1}_T \boldsymbol{\alpha}(\mathbf{X}_l, \mathbf{X})^\top \{ \mathbf{Z}_l + \xi I(\mathbf{X}_l = \mathbf{X}_u) \mathbf{e}_j \} \mathbf{1}_p^\top \right\}}{\partial \xi} \Big|_{\xi=0} \\ &= \sum_{q=1}^p \sum_{t=1}^T \frac{\partial g \left\{ \sum_{l=1}^d \mathbf{X}_l \boldsymbol{\alpha}(\mathbf{X}_l, \mathbf{X})^\top + \mathbf{1}_T \boldsymbol{\alpha}(\mathbf{X}_l, \mathbf{X})^\top \mathbf{Z}_l \mathbf{1}_p^\top \right\}}{\partial \left\{ \sum_{l=1}^d \mathbf{X}_l \boldsymbol{\alpha}(\mathbf{X}_l, \mathbf{X})^\top + \mathbf{1}_T \boldsymbol{\alpha}(\mathbf{X}_l, \mathbf{X})^\top \mathbf{Z}_l \mathbf{1}_p^\top \right\}_{qt}} \sum_{l=1}^d \boldsymbol{\alpha}(\mathbf{X}_l, \mathbf{X})^\top \mathbf{e}_j I(\mathbf{X}_l = \mathbf{X}_u) \end{aligned}$$

$$= \sum_{q=1}^p \sum_{t=1}^T \frac{\partial g \left\{ \sum_{l=1}^d \mathbf{X}_l \boldsymbol{\alpha}(\mathbf{X}_l, \mathbf{X})^\top + \mathbf{1}_T \boldsymbol{\alpha}(\mathbf{X}_l, \mathbf{X})^\top \mathbf{Z}_l \mathbf{1}_p^\top \right\}}{\partial \left\{ \sum_{l=1}^d \mathbf{X}_l \boldsymbol{\alpha}(\mathbf{X}_l, \mathbf{X})^\top + \mathbf{1}_T \boldsymbol{\alpha}(\mathbf{X}_l, \mathbf{X})^\top \mathbf{Z}_l \mathbf{1}_p^\top \right\}_{qt}} \alpha_j(\mathbf{X}_u, \mathbf{X}).$$

The same follows for the right-hand side, and hence we have

$$\sum_{q=1}^p \sum_{t=1}^T \frac{\partial g\{\mathbf{S}(\boldsymbol{\alpha})\}}{\partial S_{qt}(\boldsymbol{\alpha})} \alpha_j(\mathbf{X}_u, \mathbf{X}) = \sum_{q=1}^p \sum_{t=1}^T \frac{\partial \tilde{g}\{\mathbf{S}(\tilde{\boldsymbol{\alpha}})\}}{\partial S_{qt}(\tilde{\boldsymbol{\alpha}})} \tilde{\alpha}_j(\mathbf{X}_u, \mathbf{X}).$$

Now summing across \mathbf{u} , noting that $\partial g\{\mathbf{S}(\boldsymbol{\alpha})\}/\partial S_{qt}(\boldsymbol{\alpha})$, $\partial \tilde{g}\{\mathbf{S}(\tilde{\boldsymbol{\alpha}})\}/\partial S_{qt}(\tilde{\boldsymbol{\alpha}})$ do not contain \mathbf{X}_u , and $\sum_{u=1}^d \alpha_j(\mathbf{X}_u, \mathbf{X}) = \sum_{u=1}^d \tilde{\alpha}_j(\mathbf{X}_u, \mathbf{X}) = 1$ by our assumption, we obtain

$$\sum_{q=1}^p \sum_{t=1}^T \frac{\partial g\{\mathbf{S}(\boldsymbol{\alpha})\}}{\partial S_{qt}(\boldsymbol{\alpha})} = \sum_{q=1}^p \sum_{t=1}^T \frac{\partial \tilde{g}\{\mathbf{S}(\tilde{\boldsymbol{\alpha}})\}}{\partial S_{qt}(\tilde{\boldsymbol{\alpha}})}.$$

And hence we have

$$\alpha_j(\mathbf{X}_u, \mathbf{X}) = \tilde{\alpha}_j(\mathbf{X}_u, \mathbf{X}), j = 1, \dots, p,$$

for any \mathbf{X} and any \mathbf{u} . Combined with (S1), this suggests

$$g\{\mathbf{S}(\boldsymbol{\alpha})\} = \tilde{g}\{\mathbf{S}(\boldsymbol{\alpha})\},$$

for all $\mathbf{X}_l, \mathbf{Z}_l$, which implies $g = \tilde{g}$. This contradicts with the assumption. Therefore, g and $\boldsymbol{\alpha}$ are identifiable.

S4 Necessary Definitions and Conditions

Let $\boldsymbol{\psi}_\alpha = \{\psi_{\alpha_k}, k = 1, \dots, p\}^\top$. Furthermore, let $\boldsymbol{\alpha}^{(-k)} = (\alpha_1, \dots, \alpha_{k-1}, \alpha_{k+1}, \dots, \alpha_p)$ and

$$\begin{aligned} & \Omega(g_0, \boldsymbol{\alpha}_0, \psi_g, \boldsymbol{\psi}_\alpha, \epsilon_g^\dagger, \boldsymbol{\epsilon}_\alpha^\dagger) \\ = & \left\{ \frac{\partial^2 \mathcal{L}(g_0 + \epsilon_g \psi_g, \boldsymbol{\alpha})}{\partial \epsilon_g^2} + 2 \sum_{k=1}^p \frac{\partial^2 \mathcal{L}(g_0 + \epsilon_g \psi_g, \alpha_{0k} + \epsilon_{\alpha_k} \psi_{\alpha_k}, \boldsymbol{\alpha}^{(-k)})}{\partial \epsilon_g \partial \epsilon_{\alpha_k}} \right. \\ & \left. + \sum_{k=1}^p \sum_{j=1}^p \frac{\partial^2 \mathcal{L}(g_0, \alpha_{01}, \dots, \alpha_{0l} + \epsilon_{\alpha_l} \psi_{\alpha_l}, \dots, \alpha_{0u} + \epsilon_{\alpha_u} \psi_{\alpha_u}, \dots, \alpha_{0p})}{\partial \epsilon_{\alpha_j} \partial \epsilon_{\alpha_u}} \right\} \Big|_{\epsilon_g = \epsilon_g^\dagger, \epsilon_{\alpha_k} = \epsilon_{\alpha_k}^\dagger, k=1, \dots, p}, \end{aligned}$$

where $\epsilon_g^\dagger, \epsilon_{\alpha_k}^\dagger \in (0, 1), k = 1, \dots, p$ and $\boldsymbol{\epsilon}_\alpha^\dagger = (\epsilon_{\alpha_k}^\dagger, k = 1, \dots, p)^\top$. Define the rates

$$\phi_{\omega_j n} \equiv \max_{i=0, \dots, q_{\omega_j}} n^{-\frac{2\beta_{\omega_j i}^*}{2\beta_{\omega_j i}^* + t_{\omega_j i}}}, \phi_{gn} \equiv \max_{i=0, \dots, q_g} n^{-\frac{2\beta_{gi}^*}{2\beta_{gi}^* + t_{gi}}}, \quad (\text{S2})$$

where $\beta_{\omega_j i}^* \equiv \beta_{\omega_j i} \prod_{l=i+1}^{q_{\omega_j}} \{\min(\beta_{\omega_j l}, 1)\}$ and $\beta_{gi}^* \equiv \beta_{gi} \prod_{l=i+1}^{q_g} \{\min(\beta_{gl}, 1)\}$. Then we present the necessary conditions to guarantee the convergence of the estimators.

(C1) Assume $F_{\omega_j} \geq \max(K_{\omega_j}, 1), j = 1, \dots, p$ and $F_g \geq \max(K_g, 1)$.

(C2) Assume $\sum_{i=0}^{q_{\omega_j}} \log_2 \{\max(4t_{\omega_j i}, 4\beta_{\omega_j i})\} \log_2 n \leq L_{\omega_j} \lesssim n\phi_{\omega_j n}, j = 1, \dots, p$,

and $\sum_{i=0}^{q_g} \log_2 \{\max(4t_{gi}, 4\beta_{gi})\} \log_2 n \leq L_g \lesssim n\phi_{gn}$.

(C3) Assume $n\phi_{\omega_j n} \lesssim \min_{u=1, \dots, L} p_{\omega_j u}, j = 1, \dots, p$ and $n\phi_{gn} \lesssim \min_{u=1, \dots, L_g} p_{gu}$.

(C4) Assume $s_{\omega_j} \asymp n\phi_{\omega_j n} \log n, j = 1, \dots, p$ and $s_g \asymp n\phi_{gn} \log n$. And assume $(s_g/L_g)^{L_g/2} \leq M_L < \infty$.

(C5) Assume $|X_{ilt}|, |Z_{ilj}| \leq \max(K_{\omega_j}, K_g, j = 1, \dots, p) \leq C_M$.

(C6) Assume that

$$\begin{aligned} & 0 < \alpha_{\min} E \left[\psi_g \{\mathbf{S}_i(\boldsymbol{\alpha}_0)\}^2 + \sum_{j=1}^p \sum_{l=1}^d T \psi_{\alpha_j}(\mathbf{X}_{il}, \mathbf{X}_i)^2 \right] \\ & \leq \inf_{\epsilon_g, \boldsymbol{\epsilon}_\alpha} E \{ \Omega(g_0, \boldsymbol{\alpha}_0, \psi_g, \boldsymbol{\psi}_\alpha, \epsilon_g, \boldsymbol{\epsilon}_\alpha) \} \leq \sup_{\epsilon_g, \boldsymbol{\epsilon}_\alpha} E \{ \Omega(g_0, \boldsymbol{\alpha}_0, \psi_g, \boldsymbol{\psi}_\alpha, \epsilon_g, \boldsymbol{\epsilon}_\alpha) \} \\ & \leq \alpha_{\max} E \left[\psi_g \{\mathbf{S}_i(\boldsymbol{\alpha}_0)\}^2 + \sum_{j=1}^p \sum_{l=1}^d T \psi_{\alpha_j}(\mathbf{X}_{il}, \mathbf{X}_i)^2 \right] < \infty. \end{aligned}$$

Conditions (C1)–(C4) are standard assumptions to ensure that a deep learning network can approximate the true function with an error that vanishes as the sample size increases, as shown in Lemma S2. Condition (C5) requires bounded predictors, which are easily met in real data. Condition (C6) is commonly assumed to ensure estimation consistency under the generalized linear model.

S5 Proof of Lemma 1

Proof: First note that

$$\begin{aligned}
\alpha_j(\mathbf{x}_l, \mathbf{x}) - \alpha_{0j}(\mathbf{x}_l, \mathbf{x}) &= \frac{\exp(\omega_j(\mathbf{x}_l))}{\sum_{l=1}^d \exp(\omega_j(\mathbf{x}_l))} - \frac{\exp(\omega_{0j}(\mathbf{x}_l))}{\sum_{l=1}^d \exp(\omega_{0j}(\mathbf{x}_l))} \\
&= \frac{\exp(\omega_j^\dagger(\mathbf{x}_l))}{\sum_{l=1}^d \exp(\omega_j^\dagger(\mathbf{x}_l))} \left\{ \left(1 - \frac{\exp(\omega_j^\dagger(\mathbf{x}_l))}{\sum_{l=1}^d \exp(\omega_j^\dagger(\mathbf{x}_l))} \right) \{\omega_j(\mathbf{x}_l) - \omega_{0j}(\mathbf{x}_l)\} \right. \\
&\quad \left. - \sum_{u \neq l} \frac{\exp(\omega_j^\dagger(\mathbf{x}_u))}{\sum_{l=1}^d \exp(\omega_j^\dagger(\mathbf{x}_l))} \{\omega_j(\mathbf{x}_u) - \omega_{0j}(\mathbf{x}_u)\} \right\},
\end{aligned}$$

where ω_j^\dagger is one the line between ω_0 and ω_j , which implies

$$\sup_{\mathbf{X}_{il}, \mathbf{X}_i} |\alpha_j(\mathbf{X}_{il}, \mathbf{X}_i) - \alpha_{0j}(\mathbf{X}_{il}, \mathbf{X}_i)| \leq 2 \sup_{\mathbf{X}_{il}} |\{\omega_j(\mathbf{X}_{il}) - \omega_{0j}(\mathbf{X}_{il})\}|.$$

Furthermore,

$$\|\nabla_{g_0} \{\mathbf{S}_i(\boldsymbol{\alpha}_0)\}\|_2 \leq \|\mathbf{W}_{gL} \mathbf{W}_{gL-1}, \dots, \mathbf{W}_{g0}\|_2 \leq \sqrt{\prod_{l=1}^L s_{gl}},$$

where $\mathbf{W}_{gl}, l = 0, \dots, L$ are the weights for constructing g_0 , and s_{gl} is the sparseness of \mathbf{W}_{gl} . By the relationship between geometric and arithmetic means, we have $\prod_{l=1}^{L_g} s_{gl} \leq (\sum_{l=1}^{L_g} s_{gl}/L_g)^{L_g}$, which leads

$$\|\nabla_{g_0} \{\mathbf{S}_i(\boldsymbol{\alpha}_0)\}\|_2 \leq (s_g/L_g)^{L_g/2} \leq M_L. \tag{S3}$$

The last inequality holds by Condition (C4). Moreover, because $\nabla_{jt} g_0 \{\mathbf{S}_i(\boldsymbol{\alpha}_0)\}$ has at most s_g nonzero elements,

$$\begin{aligned}
& \left| \sum_{j=1}^p \sum_{t=1}^T \nabla_{jt} g_0 \{\mathbf{S}_i(\boldsymbol{\alpha}_0)\} \sum_{l=1}^d (X_{ilt} + Z_{ilj}) \{\alpha_j^*(\mathbf{X}_{il}, \mathbf{X}_i)^\top - \alpha_{j0}(\mathbf{X}_{il}, \mathbf{X}_i)^\top\} \right| \\
& \leq 2C_M M_L \sqrt{d \min(s_g, Tp)} \sup_{\mathbf{X}_{i,j=1,\dots,p}} |\alpha_j^*(\mathbf{X}_{il}, \mathbf{X}_i) - \alpha_{j0}(\mathbf{X}_{il}, \mathbf{X}_i)|.
\end{aligned}$$

Therefore, by Lemma S2, we have

$$\begin{aligned}
& |h' [g^* \{\mathbf{S}_i(\boldsymbol{\alpha}^*)\}] - h' [g_0 \{\mathbf{S}_i(\boldsymbol{\alpha}_0)\}]| \\
&= \left| h'' [g^\dagger \{\mathbf{S}_i(\boldsymbol{\alpha}^\dagger)\}] [g^* \{\mathbf{S}_i(\boldsymbol{\alpha}_0)\} - g_0 \{\mathbf{S}_i(\boldsymbol{\alpha}_0)\}] + h'' [g^\dagger \{\mathbf{S}_i(\boldsymbol{\alpha}^\dagger)\}] \right. \\
&\quad \times \left. \sum_{j=1}^p \sum_{t=1}^T \nabla_j g^\dagger \{\mathbf{S}_i(\boldsymbol{\alpha}^\dagger)\} \sum_{l=1}^d (X_{ilt} + Z_{ilj}) \{\alpha_j^*(\mathbf{X}_{il}, \mathbf{X}_i)^\top - \alpha_{j0}(\mathbf{X}_{il}, \mathbf{X}_i)^\top\} \right| \\
&\leq \left\{ C_g \max_{u=0, \dots, q_g} c_g^{-\frac{\beta_{gu}^*}{t_{gu}}} n^{-\frac{\beta_{gu}^*}{2\beta_{gu}^* + t_{gu}}} + 2C_M M_L \sqrt{d \min(s_g, Tp)} \right. \\
&\quad \left. \sup_{j=1, \dots, p} C_{\omega_j} \max_{u=0, \dots, q_{\omega_j}} c_{\omega_j}^{-\frac{\beta_{\omega_j u}^*}{t_{\omega_j u}}} n^{-\frac{\beta_{\omega_j u}^*}{2\beta_{\omega_j u}^* + t_{\omega_j u}}} \right\}.
\end{aligned}$$

S6 Useful Lemmas for Theorem 1

Lemma S6 Let $\psi_{\hat{g}} = \hat{g} - g_0$ and $\psi_{\hat{\alpha}_j} = \hat{\alpha}_j - \alpha_{0j}$. Assume $\hat{\alpha}_j, \alpha_{0j} \in \mathcal{H}_j$, $\omega_j^* \in \mathcal{G}_{\omega_j}$, and $\hat{g}, g_0 \in \mathcal{F}_g$, and $g^* \in \mathcal{G}_g$ and Conditions (C1)–(C5) hold, and $T, p \leq s_g$. Then there are positive constants $C_g, C_{\omega_j}, c_g, c_{\omega_j}$, $\mathbf{C}_\omega = (C_{\omega_j}, j = 1, \dots, p)^\top$, $\mathbf{c}_\omega = (c_{\omega_j}, j = 1, \dots, p)^\top$ such that

$$\begin{aligned}
& \left| n^{-1} \sum_{i=1}^n \left\{ (Y_i - h' [g_0 \{\mathbf{S}_i(\boldsymbol{\alpha}_0)\}]) \right. \right. \\
& \quad \left. \left. \sum_{j=1}^p \sum_{t=1}^T \nabla_{jt} g_0 \{\mathbf{S}_i(\boldsymbol{\alpha}_0)\} \sum_{l=1}^d (X_{ilt} + Z_{ilj}) \psi_{\hat{h}_j}(\mathbf{X}_{il}, \mathbf{X}_i) \right\} \right| \\
&\leq 4C_M M_L \eta(C_g, \mathbf{C}_\omega, c_g, \mathbf{c}_\omega) \left(\left[dpE \left\{ \sum_{j=1}^p \sum_{l=1}^d \{\sqrt{T} \psi_{\hat{\alpha}_j}(\mathbf{X}_{il}, \mathbf{X}_i)\}^2 \right\} \right]^{1/2} \right. \\
&\quad \left. + \min(s_g, Tp)^{1/2} \{\log(n)/(cn)\}^{1/4} \right)
\end{aligned}$$

with probability greater than $1 - 6n^{-1}$. And there are positive constants $B_g, B_{\omega_j}, b_g, b_{\omega_j}$,

$\mathbf{B}_\omega = (B_{\omega_j}, j = 1, \dots, p)^\top$, $\mathbf{b}_\omega = (b_{\omega_j}, j = 1, \dots, p)^\top$ that

$$\left| n^{-1} \sum_{i=1}^n \{(Y_i - h' [g_0 \{\mathbf{S}_i(\boldsymbol{\alpha}_0)\}]) \psi_{\hat{g}} \{\mathbf{S}_i(\boldsymbol{\alpha}_0)\}\} \right|$$

$$\leq 4C_M M_L \eta(B_g, B_g, \mathbf{B}_\omega, \mathbf{b}_\omega) \left[\left(E [\psi_{\hat{g}} \{\mathbf{S}_i(\boldsymbol{\alpha}_0)\}^2] \right)^{1/2} + \{\log(n)/(cn)\}^{1/4} \right].$$

with probability greater than $1 - 6n^{-1}$.

Proof: Because $Y_i - h'[g^* \{\mathbf{S}_i(\boldsymbol{\alpha}^*)\}]$ is a sub-Gaussian random variable, by Lemma 1 that $|h'[g^* \{\mathbf{S}_i(\boldsymbol{\alpha}^*)\}] - h'[g_0 \{\mathbf{S}_i(\boldsymbol{\alpha}_0)\}]| \rightarrow 0$ almost surely. We denote

$$\tau_i = \sum_{j=1}^p \sum_{t=1}^T \nabla_{jt} g_0 \{\mathbf{S}_i(\boldsymbol{\alpha}_0)\} \sum_{l=1}^d (X_{ilt} + Z_{ilj}) \psi_{\hat{\alpha}_j}(\mathbf{X}_{il}, \mathbf{X}_i)$$

in the following proof for convenience. Therefore using the concentration inequality in Lemma S4, we have

$$\begin{aligned} & \Pr \left[\left| n^{-1} \sum_{i=1}^n \{(Y_i - h'[g_0 \{\mathbf{S}_i(\boldsymbol{\alpha}_0)\}]) - E(Y_i - h'[g_0 \{\mathbf{S}_i(\boldsymbol{\alpha}_0)\}] | \mathcal{X}_n)\} \tau_i \right| \geq t \middle| \mathcal{X}_n \right] \\ & \leq 3 \exp \left[-nct^2 / \left(16n^{-1} \sum_{i=1}^n \tau_i^2 \right) \right]. \end{aligned} \quad (\text{S4})$$

Let

$$t = \sqrt{C_0 \log(n)/(cn)} \left(n^{-1} \sum_{i=1}^n \left[\sum_{j=1}^p \sum_{t=1}^T \nabla_{jt} g_0 \{\mathbf{S}_i(\boldsymbol{\alpha}_0)\} \sum_{l=1}^d (X_{ilt} + Z_{ilj}) \psi_{\hat{\alpha}_j}(\mathbf{X}_{il}, \mathbf{X}_i) \right]^2 \right)^{1/2},$$

where $C_0 = 16$, we obtain

$$\begin{aligned} & \left| n^{-1} \sum_{i=1}^n \{(Y_i - h'[g_0 \{\mathbf{S}_i(\boldsymbol{\alpha}_0)\}]) - E(Y_i - h'[g_0 \{\mathbf{S}_i(\boldsymbol{\alpha}_0)\}] | \mathcal{X}_n)\} \tau_i \right| \\ & \leq \sqrt{C_0 \log(n)/(cn)} \left(n^{-1} \sum_{i=1}^n \tau_i^2 \right)^{1/2} \end{aligned} \quad (\text{S5})$$

with probability greater than $1 - 3n^{-1}$.

Furthermore, Lemma 1 leads to

$$\begin{aligned} & \left| n^{-1} \sum_{i=1}^n E \{(Y_i - h'[g_0 \{\mathbf{S}_i(\boldsymbol{\alpha}_0)\}]) | \mathcal{X}_n\} \tau_i \right| \\ & = \left| n^{-1} \sum_{i=1}^n \left\{ (h'[g^* \{\mathbf{S}_i(\boldsymbol{\alpha}^*)\}] - h'[g_0 \{\mathbf{S}_i(\boldsymbol{\alpha}_0)\}]) \tau_i \right\} \right| \end{aligned}$$

$$\leq \left\{ C_g \max_{u=0,\dots,q_g} c_g^{-\frac{\beta_{gu}^*}{t_{gu}}} n^{-\frac{\beta_{gu}^*}{2\beta_{gu}^*+t_{gu}}} + 2C_M M_L \sqrt{d \min(s_g, Tp)} \right. \\ \left. \sup_{j=1,\dots,p} C_{\omega_j} \max_{u=0,\dots,q_{\omega_j}} c_{\omega_j}^{-\frac{\beta_{\omega_j u}^*}{t_{\omega_j u}}} n^{-\frac{\beta_{\omega_j u}^*}{2\beta_{\omega_j u}^*+t_{\omega_j u}}} \right\} \left(n^{-1} \sum_{i=1}^n \tau_i^2 \right)^{1/2}.$$

Combine with (S5), we obtain there are positive constants $C_g, C_{\omega_j}, c_g, c_{\omega_j}$ such that

$$\left| n^{-1} \sum_{i=1}^n \left\{ (Y_i - h' [g_0 \{ \mathbf{S}_i(\boldsymbol{\alpha}_0) \}]) \tau_i \right\} \right| \\ \leq \eta(C_g, \mathbf{C}_\omega, c_g, \mathbf{c}_\omega) \left(n^{-1} \sum_{i=1}^n \tau_i^2 \right)^{1/2}, \quad (\text{S6})$$

with probability greater than $1 - 3n^{-1}$. Additionally, because $\nabla g_0 \{ \mathbf{S}_i(\boldsymbol{\alpha}_0) \}$ is s_g sparse and $\sum_{l=1}^d \hat{\alpha}_j(\mathbf{X}_{il}, \mathbf{X}_i) = \sum_{l=1}^d \alpha_{0j}(\mathbf{X}_{il}, \mathbf{X}_i) = 1$, we have

$$|\tau_i| \leq 4C_M M_L \sqrt{\min(s_g, Tp)}.$$

Therefore $\tau_i^2 / \min(s_g, Tp)$ is sub-Gaussian variable, and hence

$$\Pr \left\{ \left| n^{-1} \min(s_g, Tp)^{-1} \sum_{i=1}^n \tau_i^2 - \min(s_g, Tp)^{-1} E(\tau_i^2) \right| > t \right\} \\ \leq 3 \exp \left\{ -cnt^2 / (256C_M^4 M_L^4) \right\}.$$

Let $t = \sqrt{256M_L^4 C_M^4 \log(n) / (cn)}$, we have

$$\left| n^{-1} \sum_{i=1}^n \tau_i^2 - E(\tau_i^2) \right| \leq 16 \min(s_g, Tp) C_M^2 M_L^2 \sqrt{\log(n) / (cn)}, \quad (\text{S7})$$

with probability greater than $1 - 3/n$. Next

$$E(\tau_i^2) \leq E \left(\left[\left| \sup_{l=1,\dots,d, j=1,\dots,p} \sum_{t=1}^T \nabla_{jt} g_0 \{ \mathbf{S}_i(\boldsymbol{\alpha}_0) \} (X_{ilt} + Z_{ilj}) / \sqrt{T} \right| \right. \right. \\ \left. \left. \times \sum_{j=1}^p \sum_{l=1}^d \left| \sqrt{T} \psi_{\hat{\alpha}_j}(\mathbf{X}_{il}, \mathbf{X}_i) \right| \right]^2 \right) \\ \leq 4C_M^2 M_L^2 E \left\{ \left(\sqrt{dp} \left[\sum_{j=1}^p \sum_{l=1}^d \left\{ \sqrt{T} \psi_{\hat{\alpha}_j}(\mathbf{X}_{il}, \mathbf{X}_i) \right\}^2 \right]^{1/2} \right)^2 \right\}$$

$$= 4C_M^2 M_L^2 dpE \left[\sum_{j=1}^p \sum_{l=1}^d \left\{ \sqrt{T} \psi_{\hat{\alpha}_j}(\mathbf{X}_{il}, \mathbf{X}_i) \right\}^2 \right],$$

for a constant C_M , where the second inequality holds because

$$\begin{aligned} & \left| \sup_{l=1, \dots, d, j=1, \dots, p} \sum_{t=1}^T \nabla_{jt} g_0 \{ \mathbf{S}_i(\boldsymbol{\alpha}_0) \} (X_{ilt} + Z_{ilj}) \right| \\ & \leq 2C_M \sup_{l=1, \dots, d, j=1, \dots, p} \sum_{t=1}^T |\nabla_{jt} g_0 \{ \mathbf{S}_i(\boldsymbol{\alpha}_0) \}| \\ & \leq 2C_M \sqrt{T} \sup_{l=1, \dots, d, j=1, \dots, p} \left[\sum_{t=1}^T |\nabla_{jt} g_0 \{ \mathbf{S}_i(\boldsymbol{\alpha}_0) \}| \right]^{1/2} \\ & \leq 2C_M \sqrt{T} M_L, \end{aligned}$$

by (S3). Plugging the above inequality and (S7) to (S6), we obtain

$$\begin{aligned} & \left| n^{-1} \sum_{i=1}^n \{ (Y_i - h' [g_0 \{ \mathbf{S}_i(\boldsymbol{\alpha}_0) \}]) \tau_i \} \right| \\ & \leq \eta(C_g, \mathbf{C}_\omega, c_g, \mathbf{c}_\omega) \left(2C_M M_L \left[dpE \left\{ \sum_{j=1}^p \sum_{l=1}^d \{ \sqrt{T} \psi_{\hat{\alpha}_j}(\mathbf{X}_{il}, \mathbf{X}_i) \}^2 \right\} \right]^{1/2} \right. \\ & \quad \left. + 4C_M M_L \min(s_g, Tp)^{1/2} \{ \log(n)/(cn) \}^{1/4} \right) \\ & \leq 4C_M M_L \eta(C_g, \mathbf{C}_\omega, c_g, \mathbf{c}_\omega) \left(\left[dpE \left\{ \sum_{j=1}^p \sum_{l=1}^d \{ \sqrt{T} \psi_{\hat{\alpha}_j}(\mathbf{X}_{il}, \mathbf{X}_i) \}^2 \right\} \right]^{1/2} \right. \\ & \quad \left. + \min(s_g, Tp)^{1/2} \{ \log(n)/(cn) \}^{1/4} \right) \end{aligned}$$

with probability greater than $1 - 6n^{-1}$. Using the same arguments and realize that we obtain there are positive constants $B_g, B_{\omega_j}, b_g, b_{\omega_j}$ and realize that $\|\psi_{\hat{g}}\|_2 \leq 2C_M M_L$, we have

$$\begin{aligned} & \left| n^{-1} \sum_{i=1}^n \{ (Y_i - h' [g_0 \{ \mathbf{S}_i(\boldsymbol{\alpha}_0) \}]) \psi_{\hat{g}} \{ \mathbf{S}_i(\boldsymbol{\alpha}_0) \} \} \right| \\ & \leq 4C_M M_L \eta(B_g, \mathbf{B}_\omega, b_g, \mathbf{B}_\omega) \left[(E [\psi_{\hat{g}} \{ \mathbf{S}_i(\boldsymbol{\alpha}_0) \}^2])^{1/2} + \{ \log(n)/(cn) \}^{1/4} \right]. \end{aligned}$$

with probability greater than $1 - 6n^{-1}$. This proves the result.

Lemma S7 Assume $\hat{\alpha}_j, \alpha_{0j} \in \mathcal{H}_j$, $\omega_j^* \in \mathcal{G}_{\omega_j}$, and $\hat{g}, g_0 \in \mathcal{F}_g$, $g^* \in \mathcal{G}_g$. Furthermore, assume Condition (C1)–(C6) hold, and $d/n \rightarrow 0$ and $T/n \rightarrow 0$ and $p < \infty$. Then for given $\epsilon_g^\dagger, \epsilon_{\alpha_j}^\dagger \in (0, 1)$, $\epsilon_\alpha^\dagger = \{\epsilon_{\alpha_j}^\dagger, j = 1, \dots, p\}^\top$, we have

$$\begin{aligned} \Omega(g_0, \alpha_0, \psi_{\hat{g}}, \psi_{\hat{\alpha}}, \epsilon_g^\dagger, \epsilon_\alpha^\dagger) &\geq \alpha_{\min} E \left[\psi_{\hat{g}} \{ \mathbf{S}_i(\alpha_0) \}^2 + \sum_{j=1}^p \sum_{l=1}^d T \psi_{\hat{\alpha}_j}(\mathbf{X}_{il}, \mathbf{X}_i)^2 \right] \\ &\quad - 2TpC_1 \log^2(n) \left\{ \phi_{gn} L_g + \sum_{j=1}^p \phi_{\omega_j n} L_{\omega_j} \right\} - C_H T p / n \end{aligned}$$

with probability greater than $1 - 2 \exp \left[-n C_1 \log^2(n) \left\{ \phi_{gn} L_g + \sum_{j=1}^p \phi_{\omega_j n} L_{\omega_j} \right\} \right]$ for some constants $C_H, C_1 > 0$.

Proof: Let $\psi_{\hat{g}} = \hat{g} - g_0$, $\psi_{\hat{\alpha}_k} = \hat{\alpha}_k - \alpha_0$. First, because $\hat{g}, g_0, \hat{\alpha}_k, \alpha_0$ are bounded functions, ∇g is bounded in the sense of S3, and Y_i is bounded, and $\|\mathbf{X}_{il}\|_2 \leq C_M \sqrt{T}$ by Condition (C5), it is easy to see that every summand in $Tp^{-1} \Omega(g_0, \alpha_0, \psi_g, \psi_\alpha, \epsilon_g^\dagger, \epsilon_\alpha^\dagger)$ is a product of bounded sub-Gaussian variable, and hence sub-exponential. Therefore, by Lemma S5, for arbitrary g, α , there is a constant $c_H > 0$ such that

$$\begin{aligned} &\Pr \left\{ |(Tp)^{-1} \Omega(g_0, \alpha_0, \psi_g, \psi_\alpha, \epsilon_g^\dagger, \epsilon_\alpha^\dagger) - (Tp)^{-1} E \{ \Omega(g_0, \alpha_0, \psi_g, \psi_\alpha, \epsilon_g^\dagger, \epsilon_\alpha^\dagger) \}| > t \right\} \\ &\leq 3 \exp \{ -c_H n \min(t^2, t) \}. \end{aligned}$$

Let $\mathcal{S}_g(\delta)$ be the δ covering of \mathcal{F}_g and $\mathcal{S}_{\omega_k}(\delta)$ be the δ covering of \mathcal{F}_{ω_k} , then for some constant $C_H > 0$, we have

$$\begin{aligned} &\Pr \left\{ \sup_{g \in \mathcal{F}_g, \alpha_k \in \mathcal{H}_k} |\Omega(g_0, \alpha_0, \psi_g, \psi_\alpha, \epsilon_g^\dagger, \epsilon_\alpha^\dagger) - E \{ \Omega(g_0, \alpha_0, \psi_g, \psi_\alpha, \epsilon_g^\dagger, \epsilon_\alpha^\dagger) \}| > Tpt + C_H T p \delta \right\} \\ &\leq \Pr \left\{ \max_{g \in \mathcal{S}_g, \omega_k \in \mathcal{S}_{\omega_k}} |\Omega(g_0, \alpha_0, \psi_g, \psi_\alpha, \epsilon_g^\dagger, \epsilon_\alpha^\dagger) - E \{ \Omega(g_0, \alpha_0, \psi_g, \psi_\alpha, \epsilon_g^\dagger, \epsilon_\alpha^\dagger) \}| > Tpt \right\} \\ &\leq 2 \exp \left[-c_H n \min(t^2, t) + \log \mathcal{N} \{ \delta, \mathcal{F}_g, \|\cdot\|_\infty \} + \sum_{k=1}^p \log \mathcal{N} \{ \delta, \mathcal{F}_{\omega_k}, \|\cdot\|_\infty \} \right] \\ &\leq 2 \exp \left[-c_H n \min(t^2, t) + (s_g + 1) \log \left\{ 2^{2L_g + 5} \delta^{-1} (L + 1) p_{g0}^2 p_{gL_g + 1}^2 s_g^{2L_g} \right\} \right. \\ &\quad \left. + \sum_{k=1}^p (s_{\omega_k} + 1) \log \left\{ 2^{2L_{\omega_k} + 5} \delta^{-1} (L_g \omega_k + 1) p_{\omega_k 0}^2 p_{\omega_k L_{\omega_k} + 1}^2 s_{\omega_k}^{2L_{\omega_k}} \right\} \right] \end{aligned}$$

$$\leq 2 \exp \left[-c_H n \min(t^2, t) + (s_g + 1)L_g \log \left\{ 2s_g \delta^{-1} (L_g + 1) d^2 p^2 s_g^{2L_g} \right\} \right. \\ \left. + \sum_{k=1}^p (s_{\omega_k} + 1) \log \left\{ 2^{2L_{\omega_k} + 5} \delta^{-1} (L_{\omega_k} + 1) p_{\omega_k}^2 p_{\omega_k}^{2L_{\omega_k} + 1} s_{\omega_k}^{2L_{\omega_k}} \right\} \right].$$

Now plugging $\delta = n^{-1}$ using Condition (C2)–(C4) and the fact that $d/n \rightarrow 0$ and $T/n \rightarrow 0$

and $p < \infty$, we have

$$\Pr \left\{ \sup_{g \in \mathcal{F}_g, \alpha_k \in \mathcal{H}_k} |\Omega(g_0, \boldsymbol{\alpha}_0, \psi_g, \boldsymbol{\psi}_\alpha, \epsilon_g^\dagger, \boldsymbol{\epsilon}_\alpha^\dagger) - E\{\Omega(g_0, \boldsymbol{\alpha}_0, \psi_g, \boldsymbol{\psi}_\alpha, \epsilon_g^\dagger, \boldsymbol{\epsilon}_\alpha^\dagger)\}| > Tpt + C_H Tp/n \right\} \\ \leq 2 \exp \left[-c_H n \min(t^2, t) + c_1 n \phi_{gn} L_g \log^2(n) + \sum_{j=1}^p c_{2j} n \phi_{\omega_j n} L_{\omega_j} \log^2(n) \right].$$

Let $t = \max \left[2C_1 \log^2(n) \left\{ \phi_{gn} L_g + \sum_{j=1}^p \phi_{\omega_j n} L_{\omega_j} \log^2(n) \right\}, 1 \right]$, where $C_1 = 2\{c_1 + \max_j(c_{2j})\}/c_H$, we have

$$\Pr \left\{ \sup_{g \in \mathcal{F}_g, \alpha_k \in \mathcal{H}_k} |\Omega(g_0, \boldsymbol{\alpha}_0, \psi_g, \boldsymbol{\psi}_\alpha, \epsilon_g^\dagger, \boldsymbol{\epsilon}_\alpha^\dagger) - E\{\Omega(g_0, \boldsymbol{\alpha}_0, \psi_g, \boldsymbol{\psi}_\alpha, \epsilon_g^\dagger, \boldsymbol{\epsilon}_\alpha^\dagger)\}| \right. \\ \left. > 2TpC_1 \log^2(n) \left\{ \phi_{gn} L_g + \sum_{j=1}^p \phi_{\omega_j n} L_{\omega_j} \right\} + C_H Tp/n \right\} \\ \leq 2 \exp \left[-nC_1 \log^2(n) \left\{ \phi_{gn} L_g + \sum_{j=1}^p \phi_{\omega_j n} L_{\omega_j} \right\} \right].$$

Therefore,

$$|\Omega(g_0, \boldsymbol{\alpha}_0, \psi_{\hat{g}}, \boldsymbol{\psi}_{\hat{\alpha}}, \epsilon_{\hat{g}}^\dagger, \boldsymbol{\epsilon}_{\hat{\alpha}}^\dagger) - E\{\Omega(g_0, \boldsymbol{\alpha}_0, \psi_{\hat{g}}, \boldsymbol{\psi}_{\hat{\alpha}}, \epsilon_{\hat{g}}^\dagger, \boldsymbol{\epsilon}_{\hat{\alpha}}^\dagger)\}| \\ \leq TpC_1 \log^2(n) \left\{ \phi_{gn} L_g + \sum_{j=1}^p \phi_{\omega_j n} L_{\omega_j} \right\} + C_H Tp/n,$$

with probability greater than $1 - 2 \exp \left[-nC_1 \log^2(n) \left\{ \phi_{gn} L_g + \sum_{j=1}^p \phi_{\omega_j n} L_{\omega_j} \right\} \right]$ for some $C_1 > 0$. Hence

$$\Omega(g_0, \boldsymbol{\alpha}_0, \psi_{\hat{g}}, \boldsymbol{\psi}_{\hat{\alpha}}, \epsilon_{\hat{g}}^\dagger, \boldsymbol{\epsilon}_{\hat{\alpha}}^\dagger) \geq \alpha_{\min} E \left[\psi_{\hat{g}} \{\mathbf{S}_i(\boldsymbol{\alpha}_0)\}^2 + \sum_{j=1}^p \sum_{l=1}^d T \psi_{\hat{\alpha}_j}(\mathbf{X}_{il}, \mathbf{X}_i)^2 \right] \\ - TpC_1 \log^2(n) \left\{ \phi_{gn} L_g + \sum_{j=1}^p \phi_{\omega_j n} L_{\omega_j} \right\} - C_H Tp/n$$

with probability greater than $1 - 2 \exp \left[-nC_1 \log^2(n) \left\{ \phi_{gn} L_g + \sum_{j=1}^p \phi_{\omega_j n} L_{\omega_j} \right\} \right]$. This proves the result.

S7 Theorem S1

Below we derive the convergence rate and establish the asymptotic consistency of the estimator as a supplement to Theorem 1 in the main material. For the positive constants $C_0, A_g, A_{\omega_j}, a_g, a_{\omega_j}, j = 1, \dots, p$, we define

$$\eta(A_g, a_g, \mathbf{A}_\omega, \mathbf{a}_\omega) \equiv \sqrt{C_0 \log(n)/(cn)} + \left\{ A_g \max_{u=0, \dots, q_g} a_g^{-\frac{\beta_{gu}^*}{t_{gu}}} n^{-\frac{\beta_{gu}^*}{2\beta_{gu}^* + t_{gu}}} \right. \\ \left. + 2C_M M_L \sqrt{d \min(s_g, Tp)} \sup_{j=1, \dots, p} A_{\omega_j} \max_{u=0, \dots, q_{\omega_j}} a_{\omega_j}^{-\frac{\beta_{\omega_j u}^*}{t_{\omega_j u}}} n^{-\frac{\beta_{\omega_j u}^*}{2\beta_{\omega_j u}^* + t_{\omega_j u}}} \right\},$$

where $\mathbf{A}_\omega = (A_{\omega_j}, j = 1, \dots, p)^\top$, and $\mathbf{a}_\omega = (a_{\omega_j}, j = 1, \dots, p)^\top$.

Theorem S1 *Let $\psi_{\hat{g}} = \hat{g} - g_0$ and $\psi_{\hat{\alpha}_j} = \hat{\alpha}_j - \alpha_{0j}$. Assume $\hat{\alpha}_j, \alpha_{0j} \in \mathcal{H}_j$, $\omega_j^* \in \mathcal{G}_{\omega_j}$, $\hat{g}, g_0 \in \mathcal{F}_g$, and $g^* \in \mathcal{G}_g$. Assume $T, p < s_g$ and Conditions (C1)–(C6) hold. Let $dP_{\alpha}(\cdot)$ be the probability density function of $\mathbf{S}_i(\alpha)$, and assume $\|dP_{\alpha_0}(\mathbf{z})/dP_{\alpha^*}(\mathbf{z})\|_\infty \geq m_h > 0$. Furthermore, let $dP_{\mathbf{X}}(\cdot)$ be the probability density for \mathbf{X}_i . Then there are positive constants $D_g, d_g, \mathbf{D}_\omega = (D_{\omega_j}), \mathbf{d}_\omega = (d_{\omega_j}), D_{g1}, d_{g1}, D_{\omega_j1}, d_{\omega_j1}, c'_H, C_H$ such that*

$$\int \{\hat{g}(\mathbf{z}) - g^*(\mathbf{z})\}^2 dP_{\alpha^*}(\mathbf{z}) + \sum_{j=1}^p \int \sum_{l=1}^d \{\hat{\alpha}_j(\mathbf{x}_l, \mathbf{x}) - \alpha_j^*(\mathbf{x}_l, \mathbf{x})\}^2 dP_{\mathbf{X}}(\mathbf{x}) \\ \leq 16 \min(m_h, 1)^{-1} \alpha_{\min}^{-1} \left(C_M M_L \eta(D_g, d_g, \mathbf{D}_\omega, \mathbf{d}_\omega) \left[\min(s_g, Tp)^{1/2} \{\log(n)/(cn)\}^{1/4} \right. \right. \\ \left. \left. + \{\log(n)/(cn)\}^{1/4} \right] + Tp C_1 \log^2(n) \left\{ \phi_{gn} L_g + \sum_{j=1}^p \phi_{\omega_j n} L_{\omega_j} \right\} + C_H Tp/n \right) \\ + 32 \min(m_h, 1)^{-1} C_M M_L d p \alpha_{\min}^{-2} \eta(D_g, d_g, \mathbf{D}_\omega, \mathbf{d}_\omega)^2 + \left(D_{g1} \phi_{gn} + T \sum_{j=1}^p D_{\omega_j1} \phi_{\omega_j n} \right)$$

with probability greater than $1 - 6n^{-1} - 2 \exp \left[-n C_1 \log^2(n) \left\{ \phi_{gn} L_g + \sum_{j=1}^p \phi_{\omega_j n} L_{\omega_j} \right\} \right]$.

When $n \rightarrow \infty$ and T, p are finite, we have

$$\int \{\hat{g}(\mathbf{z}) - g^*(\mathbf{z})\}^2 dP_{\alpha^*}(\mathbf{z}) + \sum_{j=1}^p \int \sum_{l=1}^d \{\hat{\alpha}_j(\mathbf{x}_l, \mathbf{x}) - \alpha_j^*(\mathbf{x}_l, \mathbf{x})\}^2 dP_{\mathbf{X}}(\mathbf{x}) \xrightarrow{P} 0.$$

The upper bound of the error is dominated by $TpC_1 \log^2(n) \left\{ \phi_{gn}L_g + \sum_{j=1}^p \phi_{\omega_j n}L_{\omega_j} \right\}$ when T and p are finite. Also because ϕ_{gn} and $\phi_{\omega_j n}$ are of the order of the inverse of polynomial functions of n , the upper bound approaches zero with the probability increasing to one as the sample size $n \rightarrow \infty$. This shows that the error converges to zero in probability.

S8 Proof of Theorem S1

Proof: Because \widehat{g} , $\widehat{\boldsymbol{\alpha}}$ is the minimizer of (4), we have

$$\begin{aligned}
0 &\geq \mathcal{L}(\widehat{g}, \widehat{\boldsymbol{\alpha}}) - \mathcal{L}(g_0, \boldsymbol{\alpha}_0) \\
&= -n^{-1} \sum_{i=1}^n \left\{ (Y_i - h' [g_0 \{ \mathbf{S}_i(\boldsymbol{\alpha}_0) \}]) \right. \\
&\quad \left. \sum_{j=1}^p \sum_{t=1}^T \nabla_{jt} g_0 \{ \mathbf{S}_i(\boldsymbol{\alpha}_0) \} \sum_{l=1}^d (X_{ilt} + Z_{ilj}) \psi_{\widehat{\alpha}_j}(\mathbf{X}_{il}, \mathbf{X}_i) \right\} \\
&\quad - n^{-1} \sum_{i=1}^n [(Y_i - h' [g_0 \{ \mathbf{S}_i(\boldsymbol{\alpha}_0) \}]) \psi_{\widehat{g}} \{ \mathbf{S}_i(\boldsymbol{\alpha}_0) \}] \\
&\quad + \Omega(g_0, \boldsymbol{\alpha}_0, \psi_{\widehat{g}}, \boldsymbol{\psi}_{\widehat{\boldsymbol{\alpha}}}, \boldsymbol{\epsilon}_g^\dagger, \boldsymbol{\epsilon}_\alpha^\dagger) / 2,
\end{aligned}$$

where $\boldsymbol{\epsilon}_g^\dagger, \boldsymbol{\epsilon}_{\alpha_j}^\dagger \in (0, 1)$ and $\boldsymbol{\epsilon}_\alpha^\dagger = (\boldsymbol{\epsilon}_{\alpha_j}^\dagger, j = 1, \dots, p)^\top$. By Lemma S6 and S7, we have there are positive constants $D_g, d_g, \mathbf{D}_\omega = (D_{\omega_j}), \mathbf{d}_\omega = (d_{\omega_j})$ such that

$$\begin{aligned}
&4C_M M_L \eta(D_g, d_g, \mathbf{D}_\omega, \mathbf{d}_\omega) \left[\left[dpE \left\{ \sum_{j=1}^p \sum_{l=1}^d T \psi_{\widehat{\alpha}_j}(\mathbf{X}_{il}, \mathbf{X}_i)^2 \right\} \right]^{1/2} \right. \\
&+ (E [\psi_{\widehat{g}} \{ \mathbf{S}_i(\boldsymbol{\alpha}_0) \}^2])^{1/2} \left. \right] + 4C_M M_L \eta(D_g, d_g, \mathbf{D}_\omega, \mathbf{d}_\omega) \left[\min(s_g, Tp)^{1/2} \{ \log(n)/(cn) \}^{1/4} \right. \\
&+ \{ \log(n)/(cn) \}^{1/4} \left. \right] + TpC_1 \log^2(n) \left\{ \phi_{gn}L_g + \sum_{j=1}^p \phi_{\omega_j n}L_{\omega_j} \right\} / 2 + C_H Tp / (2n) \\
&\geq \alpha_{\min} E \left[\psi_{\widehat{g}} \{ \mathbf{S}_i(\boldsymbol{\alpha}_0) \}^2 + \sum_{j=1}^p \sum_{l=1}^d T \psi_{\widehat{\alpha}_j}(\mathbf{X}_{il}, \mathbf{X}_i)^2 \right] / 2
\end{aligned}$$

with probability greater than $1 - 6n^{-1} - 2 \exp \left[-nC_1 \log^2(n) \left\{ \phi_{gn}L_g + \sum_{j=1}^p \phi_{\omega_j n}L_{\omega_j} \right\} \right]$.

This implies

$$\begin{aligned}
& 4C_M M_L \eta(D_g, d_g, \mathbf{D}_\omega, \mathbf{d}_\omega) (dp/2)^{1/2} \left(E \left\{ \sum_{j=1}^p \sum_{l=1}^d T \psi_{\hat{\alpha}_j}(\mathbf{X}_{il}, \mathbf{X}_i)^2 \right\} \right. \\
& \left. + E \left[\psi_{\hat{g}} \{ \mathbf{S}_i(\boldsymbol{\alpha}_0) \}^2 \right] \right)^{1/2} \\
& + 4C_M M_L \eta(D_g, d_g, \mathbf{D}_\omega, \mathbf{d}_\omega) \left[\min(s_g, Tp)^{1/2} \{ \log(n)/(cn) \}^{1/4} + \{ 16 \log(n)/(cn) \}^{1/4} \right] \\
& + TpC_1 \log^2(n) \left\{ \phi_{gn}L_g + \sum_{j=1}^p \phi_{\omega_j n}L_{\omega_j} \right\} / 2 + C_H Tp / (2n) \\
& \geq \alpha_{\min} E \left[\psi_{\hat{g}} \{ \mathbf{S}_i(\boldsymbol{\alpha}_0) \}^2 + \sum_{j=1}^p \sum_{l=1}^d T \psi_{\hat{\alpha}_j}(\mathbf{X}_{il}, \mathbf{X}_i)^2 \right] / 2.
\end{aligned}$$

Therefore, we have

$$\begin{aligned}
& E \left[\psi_{\hat{g}} \{ \mathbf{S}_i(\boldsymbol{\alpha}_0) \}^2 + \sum_{j=1}^p \sum_{l=1}^d T \psi_{\hat{\alpha}_j}(\mathbf{X}_{il}, \mathbf{X}_i)^2 \right] \\
& \leq 16\alpha_{\min}^{-1} \left(C_M M_L \eta(D_g, d_g, \mathbf{D}_\omega, \mathbf{d}_\omega) \left[\min(s_g, Tp)^{1/2} \{ \log(n)/(cn) \}^{1/4} + \{ \log(n)/(cn) \}^{1/4} \right] \right. \\
& \left. + TpC_1 \log^2(n) \left\{ \phi_{gn}L_g + \sum_{j=1}^p \phi_{\omega_j n}L_{\omega_j} \right\} / 2 + C_H Tp / (2n) \right) \\
& + 32C_M M_L dp \alpha_{\min}^{-2} \eta(D_g, d_g, \mathbf{D}_\omega, \mathbf{d}_\omega)^2.
\end{aligned}$$

Now because $\|dP_{\alpha_0}(\mathbf{z})/dP_{\alpha^*}(\mathbf{z})\|_\infty \geq m_h$ almost surely, we obtain

$$\begin{aligned}
& E \left[\psi_{\hat{g}} \{ \mathbf{S}_i(\boldsymbol{\alpha}^*) \}^2 + \sum_{j=1}^p \sum_{l=1}^d T \psi_{\hat{\alpha}_j}(\mathbf{X}_{il}, \mathbf{X}_i)^2 \right] \\
& \leq 16 \min(m_h, 1)^{-1} \alpha_{\min}^{-1} \left(C_M M_L \eta(D_g, d_g, \mathbf{D}_\omega, \mathbf{d}_\omega) \left[\min(s_g, Tp)^{1/2} \{ \log(n)/(cn) \}^{1/4} \right. \right. \\
& \left. \left. + \{ \log(n)/(cn) \}^{1/4} \right] + TpC_1 \log^2(n) \left\{ \phi_{gn}L_g + \sum_{j=1}^p \phi_{\omega_j n}L_{\omega_j} \right\} + C_H Tp/n \right) \\
& + 32 \min(m_h, 1)^{-1} C_M M_L dp \alpha_{\min}^{-2} \eta(D_g, d_g, \mathbf{D}_\omega, \mathbf{d}_\omega)^2.
\end{aligned}$$

Now again using Lemma S2, we obtain there are constants D_{g1}, D_{ω_j1} such that

$$\int \{ \hat{g}(\mathbf{z}) - g^*(\mathbf{z}) \}^2 dP_{\alpha^*}(\mathbf{z}) + T \sum_{j=1}^p \int \sum_{l=1}^d \{ \hat{\alpha}_j(\mathbf{x}_l, \mathbf{x}) - \alpha_j^*(\mathbf{x}_l, \mathbf{x}) \}^2 dP_{\mathbf{X}}(\mathbf{x})$$

$$\begin{aligned}
&\leq 16 \min(m_h, 1)^{-1} \alpha_{\min}^{-1} \left(C_M M_L \eta(D_g, d_g, \mathbf{D}_\omega, \mathbf{d}_\omega) \left[\min(s_g, Tp)^{1/2} \{\log(n)/(cn)\}^{1/4} \right. \right. \\
&\quad \left. \left. + \{\log(n)/(cn)\}^{1/4} \right] + Tp C_1 \log^2(n) \left\{ \phi_{gn} L_g + \sum_{j=1}^p \phi_{\omega_j n} L_{\omega_j} \right\} + C_H Tp/n \right) \\
&\quad + 32 \min(m_h, 1)^{-1} C_M M_L dp \alpha_{\min}^{-2} \eta(D_g, d_g, \mathbf{D}_\omega, \mathbf{d}_\omega)^2 + \left(D_{g1} \phi_{gn} + T \sum_{j=1}^p D_{\omega_j 1} \phi_{\omega_j n} \right)
\end{aligned}$$

with probability greater than $1 - 6n^{-1} - 2 \exp \left[-nC_1 \log^2(n) \left\{ \phi_{gn} L_g + \sum_{j=1}^p \phi_{\omega_j n} L_{\omega_j} \right\} \right]$.

This proves the result.

S9 Examples of Theorem S1

We discuss the convergence rates under special cases of g , ω_k , $k = 1, \dots, p$. This discussion is similar to Section 4 in Schmidt-Hieber (2020).

Additive model: Assume that ω_k , $k = 1, \dots, p$ has the form

$$\omega_k(\mathbf{x}) = \sum_{t=1}^T \omega_{kt}(x_t).$$

This can be written as a composition of functions

$$\omega_k = \omega_{1k} \circ \omega_{0k}$$

where $\omega_{0k}(\mathbf{x}) = (\omega_{0k1}(x_1), \dots, \omega_{0kT}(x_T))^\top$ and $\omega_{1k}(\mathbf{y}) = \sum_{t=1}^T y_t$. Then $\omega_{0k} : [-1, 1]^T \rightarrow \mathbb{R}^T$ and $\omega_{1k} : \mathbb{R}^T \rightarrow \mathbb{R}$. Thus, for $\omega_k \in \mathcal{G}_{\omega_k}$ we have $q_{\omega_k} = 1$, $\mathbf{d}_{\omega_k} = (d_0, d_1, d_2) = (T, T, 1)$, and $\mathbf{t}_{\omega_k} = (t_0, t_1) = (1, T)$. Suppose $\omega_{kt} \in \mathcal{C}_1^\beta([-1, 1], K)$ for $t = 1, \dots, T$. Then $\omega_k : [-1, 1]^T \xrightarrow{\omega_{0k}} [-K, K]^T \xrightarrow{\omega_{1k}} [-KT, KT]$. Since for any $\beta_1 > 1$, $\omega_{1k} \in \mathcal{C}_T^{\beta_1}([-K, K]^T, (K + 1)T)$, then $\phi_{\omega_j n} = n^{-\frac{2\beta}{2\beta+1}}$ and

$$\omega_k \in \mathcal{G}(1, (T, T, 1), (1, T), (\beta, \max(\beta, 2)T), (K + 1)T).$$

Similarly, assume that g has the form

$$g(\mathbf{z}) = \sum_{k=1}^p \sum_{j=1}^T g_{jk}(z_{jk}).$$

This can be written as a composition of functions

$$g = g_1 \circ g_0$$

where $g_0(\mathbf{z}) = (g_{jk}(z_{jk}), j = 1, \dots, T; k = 1, \dots, p)_{T \times p}$ and $g_1(\mathbf{y}) = \sum_{k=1}^p \sum_{j=1}^T y_{jk}$. Thus for $g \in \mathcal{G}_g$ we have $q_g = 1$, $\mathbf{d}_g = (d_0, d_1, d_2) = (Tp, Tp, 1)$, and $\mathbf{t}_g = (t_0, t_1) = (1, Tp)$. Suppose $g_{jk} \in \mathcal{C}_1^\beta([-d, d], K)$ for $j = 1, \dots, T$ and $k = 1, \dots, p$. Then $g : [-d, d]^{T \times p} \xrightarrow{g_0} [-K, K]^{T \times p} \xrightarrow{g_1} [-K Tp, K Tp]$. Thus, $\phi_{gn} = n^{-\frac{2\beta}{2\beta+1}}$ and

$$g \in \mathcal{G}(1, (Tp, Tp, 1), (1, Tp), (\beta, \max(\beta, 2)Tp), (K + 1)Tp).$$

Then for network architectures $\mathcal{F}_{\omega_j}, \mathcal{F}_g$ with $L_{\omega_j n} \lesssim \log n$, $L_g \lesssim \log n$ satisfying Conditions (C1)–(C4), we have $F_{\omega_j} \geq (K + 1)T$, $F_g \geq (K + 1)Tp$, $2 \log_2(4 \max(\beta, 2)T) \log n \leq L_{\omega_j} \lesssim \log n$, $2 \log_2(4 \max(\beta, 2)Tp) \log n \leq L_g \lesssim \log n$, $n^{1/(2\beta+1)} \lesssim \min_u p_{\omega_j u}, j = 1, \dots, p$, $n^{1/(2\beta+1)} \lesssim \min_u p_{gu}$, $s_{\omega_j} \asymp n^{1/(2\beta+1)} \log n$, $s_g \asymp n^{1/(2\beta+1)} \log n$. Through Theorem S1, under Conditions (C1)–(C6), we obtain

$$Tp C_1 \log^2(n) \left\{ \phi_{gn} L_g + \sum_{j=1}^p \phi_{\omega_j n} L_{\omega_j} \right\} \lesssim Tp(p + 1) C_1 n^{-\frac{2\beta}{2\beta+1}} \log^3 n.$$

This shows that the estimators converge at least at the rate $\log^3 n$.

S10 Simluation

We evaluate NDL using simulation studies with different sample sizes n to examine the convergence of the estimation procedure.

To simulate data that closely resemble real-world conditions, we randomly segment $d \times (T + p)$ brain signal matrices from the TUH data, with $d = 22$, $T = 64$ and $p = 64$. Each matrix is standardized by subtracting the mean of its rows and dividing by the standard deviation of its elements. We then extract the segment between the $(p/2 + 1)$ th column

and the $(p/2 + T)$ th column as \mathbf{X}_i , forming a $d \times T$ matrix. The remaining columns are used as \mathbf{Z}_i , a $d \times p$ matrix. We choose the true functions $\omega_k^*(\mathbf{X}_{il})$, $k = 1, \dots, p$, randomly with replacement from the following set:

$$\left\{ \log \left(\sum_{t=1}^T (X_{ilt})^2 / T - \mu_{il}^2 \right), -\log \left(\sum_{t=1}^T (X_{ilt})^2 / T - \mu_{il}^2 \right), \right. \\ \left. \left(\sum_{t=1}^T (z_{ilt})^3 / T \right), - \left(\sum_{t=1}^T (z_{ilt})^3 / T \right), \left(\sum_{t=1}^T (z_{ilt})^4 / T - 3 \right), - \left(\sum_{t=1}^T (z_{ilt})^4 / T - 3 \right), \right. \\ \left. \log \left(\sum_{t=1}^T |X_{ilt} \sin(X_{ilt})| \right), \log \left(\sum_{t=1}^T |X_{ilt} \cos(X_{ilt})| \right) \right\},$$

where $z_{ilt} = (X_{ilt} - \mu_{il}) / \sigma_{il}$ with $\mu_{il} = \sum_{t=1}^T X_{ilt} / T$ and $\sigma_{il} = \sqrt{\sum_{t=1}^T (X_{ilt})^2 / T - \mu_{il}^2}$. Furthermore, we generate $\boldsymbol{\beta}_1 = (\beta_{11}, \dots, \beta_{1T})^\top$ and $\boldsymbol{\beta}_2 = (\beta_{21}, \dots, \beta_{2p})^\top$ from the standard multivariate normal distributions and β_0 from the standard normal distribution. The coefficient parameters $\{\beta_0, \boldsymbol{\beta}_1, \boldsymbol{\beta}_2\}$ are fixed for all simulation repetitions. Finally, we define $g^* \{\mathbf{S}_i(\boldsymbol{\alpha}^*)\} = \boldsymbol{\beta}_1^\top \mathbf{S}_i(\boldsymbol{\alpha}^*) \boldsymbol{\beta}_2 + \beta_0$, and sample Y_i as a Bernoulli variable with the probability of success being $(\exp[-g^* \{\mathbf{S}_i(\boldsymbol{\alpha}^*)\}] + 1)^{-1}$.

We apply NDL to each simulated sample set $\{(\mathbf{X}_i, \mathbf{Z}_i, Y_i), i = 1, \dots, n\}$ and obtain the resulting estimators $\hat{\boldsymbol{\alpha}}, \hat{g}$. Then we measure the estimation errors of $\hat{\boldsymbol{\alpha}}$ and \hat{g} , respectively:

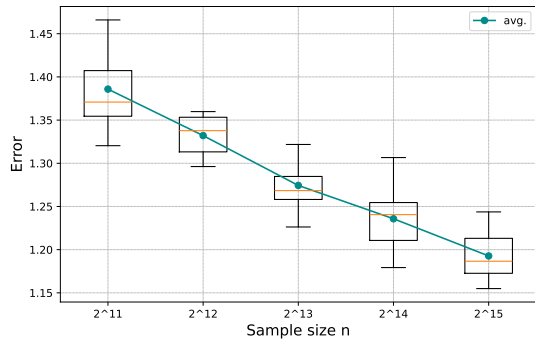
$$d_{\boldsymbol{\alpha}^*}(\hat{\boldsymbol{\alpha}}) = \frac{1}{N} \sum_{i=1}^N \left\| \{\hat{\boldsymbol{\alpha}}(\mathbf{X}_{il}, \mathbf{X}_i), l = 1, \dots, d\}^\top - \{\boldsymbol{\alpha}^*(\mathbf{X}_{il}, \mathbf{X}_i), l = 1, \dots, d\}^\top \right\|_2,$$

and

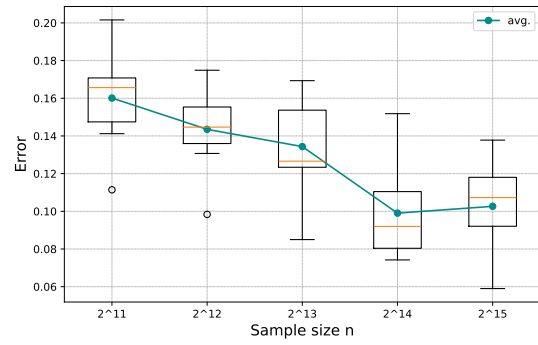
$$d_{g^*}(\hat{g}) = \frac{1}{N} \sum_{i=1}^N |h'[\hat{g}\{\mathbf{S}_i(\hat{\boldsymbol{\alpha}})\}] - h'[g^*\{\mathbf{S}_i(\hat{\boldsymbol{\alpha}})\}]|,$$

where $N = 4096$ samples are randomly selected from simulated data to evaluate the estimation errors of the functions.

We generate data for five settings of varying sample sizes $n_j = 2^{10+j}$, $j = 1, \dots, 5$. Each setting is repeated 10 times. Figure S1 shows that $d_{\boldsymbol{\alpha}^*}(\hat{\boldsymbol{\alpha}})$ and $d_{g^*}(\hat{g})$ decrease as the sample size n increases. One can see that both $\boldsymbol{\alpha}(\mathbf{X}_{il}, \mathbf{X}_i)$ and $g\{\mathbf{S}_i(\boldsymbol{\alpha})\}$ are identifiable and our estimators converge to the true values as the sample size increases.



(a) $d_{\alpha^*}(\hat{\alpha})$



(b) $d_{g^*}(\hat{g})$

Figure S1: Boxplots of the estimation errors under different sample sizes over 10 repetitions.

S11 The Standard ACNS Temporal Central Parasagittal (TCP) Montage

Table S1: The standard ACNS TCP montage.

Index	Montage	Anode	Cathode
0	FP1-F7	EEG FP1-REF	EEG F7-REF
1	F7-T3	EEG F7-REF	EEG T3-REF
2	T3-T5	EEG T3-REF	EEG T5-REF
3	T5-O1	EEG T5-REF	EEG O1-REF
4	FP2-F8	EEG FP2-REF	EEG F8-REF
5	F8-T4	EEG F8-REF	EEG T4-REF
6	T4-T6	EEG T4-REF	EEG T6-REF
7	T6-O2	EEG T6-REF	EEG O2-REF
8	A1-T3	EEG A1-REF	EEG T3-REF
9	T3-C3	EEG T3-REF	EEG C3-REF
10	C3-CZ	EEG C3-REF	EEG CZ-REF
11	CZ-C4	EEG CZ-REF	EEG C4-REF
12	C4-T4	EEG C4-REF	EEG T4-REF
13	T4-A2	EEG T4-REF	EEG A2-REF
14	FP1-F3	EEG FP1-REF	EEG F3-REF
15	F3-C3	EEG F3-REF	EEG C3-REF
16	C3-P3	EEG C3-REF	EEG P3-REF
17	P3-O1	EEG P3-REF	EEG O1-REF
18	FP2-F4	EEG FP2-REF	EEG F4-REF
19	F4-C4	EEG F4-REF	EEG C4-REF
20	C4-P4	EEG C4-REF	EEG P4-REF
21	P4-O2	EEG P4-REF	EEG O2-REF

References

- Antoniades, A., Spyrou, L., Took, C. C., and Sanei, S. (2016), “Deep learning for epileptic intracranial eeg data”, in *2016 IEEE 26th International Workshop on Machine Learning for Signal Processing (MLSP)*, pp. 1–6, DOI: 10.1109/MLSP.2016.7738824.
- Baud, M. O., Kleen, J. K., Anumanchipalli, G. K., Hamilton, L. S., Tan, Y.-L., Knowlton, R., et al. (2018), “Unsupervised learning of spatiotemporal interictal discharges in focal epilepsy”, *Neurosurgery*, 83(4), 683–691, DOI: 10.1093/neuros/nyx480.
- Chung, Y. G., Lee, W.-J., Na, S. M., Kim, H., Hwang, H., Yun, C.-H., et al. (2023), “Deep learning-based automated detection and multiclass classification of focal interictal epileptiform discharges in scalp electroencephalograms”, *Scientific Reports*, 13(1), 6755, DOI: 10.1038/s41598-023-33906-5.
- Clarke, S., Karoly, P. J., Nurse, E., Seneviratne, U., Taylor, J., Knight-Sadler, R., et al. (2021), “Computer-assisted eeg diagnostic review for idiopathic generalized epilepsy”, *Epilepsy & Behavior*, 121, 106556, DOI: 10.1016/j.yebeh.2019.106556.
- Ester, M., Kriegel, H.-P., Sander, J., and Xu, X. (1996), “A density-based algorithm for discovering clusters in large spatial databases with noise”, in *Proceedings of the Second International Conference on Knowledge Discovery and Data Mining, KDD’96*, AAAI Press, pp. 226–231, DOI: 10.5555/3001460.3001507.
- Goelz, H., Jones, R. D., and Bones, P. J. (2000), “Wavelet analysis of transient biomedical signals and its application to detection of epileptiform activity in the eeg”, *Clinical electroencephalography*, 31(4), 181–191, DOI: 10.1177/155005940003100406.

- Golmohammadi, M., Harati Nejad Torbati, A. H., Lopez de Diego, S., Obeid, I., and Picone, J. (2019), “Automatic analysis of eegs using big data and hybrid deep learning architectures”, *Frontiers in human neuroscience*, 13, 76, DOI: 10.3389/fnhum.2019.00076.
- Harati, A., Golmohammadi, M., Lopez, S., Obeid, I., and Picone, J. (2015), “Improved eeg event classification using differential energy”, in *2015 IEEE Signal Processing in Medicine and Biology Symposium (SPMB)*, IEEE, pp. 1–4, DOI: 10.1109/SPMB.2015.7405421.
- Imaizumi, M., and Fukumizu, K. (2019), “Deep neural networks learn non-smooth functions effectively”, in *The 22nd international conference on artificial intelligence and statistics*, PMLR, pp. 869–878. Available at <https://proceedings.mlr.press/v89/imaizumi19a.html>.
- Indiradevi, K., Elias, E., Sathidevi, P., Nayak, S. D., and Radhakrishnan, K. (2008), “A multi-level wavelet approach for automatic detection of epileptic spikes in the electroencephalogram”, *Computers in biology and medicine*, 38(7), 805–816, DOI: 10.1016/j.compbiomed.2008.04.010.
- Jacobs, R. A., Jordan, M. I., Nowlan, S. J., and Hinton, G. E. (1991), “Adaptive mixtures of local experts”, *Neural computation*, 3(1), 79–87, DOI: 10.1162/neco.1991.3.1.79.
- Jing, J., Sun, H., Kim, J. A., Herlopian, A., Karakis, I., Ng, M., et al. (2020), “Development of expert-level automated detection of epileptiform discharges during electroencephalogram interpretation”, *JAMA Neurology*, 77(1), 103–108, DOI: 10.1001/jamaneurol.2019.3485.
- Johansen, A. R., Jin, J., Maszczyk, T., Dauwels, J., Cash, S. S., and Westover, M. B. (2016), “Epileptiform spike detection via convolutional neural networks”, in *2016 IEEE International Conference on Acoustics, Speech and Signal Processing (ICASSP)*, IEEE, pp. 754–758, DOI: 10.1109/ICASSP.2016.7471776.

- Lodder, S. S., Askamp, J., and van Putten, M. J. (2013), “Inter-ictal spike detection using a database of smart templates”, *Clinical neurophysiology*, 124(12), 2328–2335, DOI: 10.1016/j.clinph.2013.05.019.
- Lopez, S., Gross, A., Yang, S., Golmohammadi, M., Obeid, I., and Picone, J. (2016), “An analysis of two common reference points for eegs”, in *2016 IEEE signal processing in medicine and biology symposium (SPMB)*, IEEE, pp. 1–5, DOI: 10.1109/SPMB.2016.7846854.
- McIntosh, W. C., and Das, J. M. (2019), *Temporal Seizure*, StatPearls. Available at <https://www.ncbi.nlm.nih.gov/books/NBK549852/>.
- Medvedev, A., Agoureeva, G., and Murro, A. (2019), “A long short-term memory neural network for the detection of epileptiform spikes and high frequency oscillations”, *Scientific reports*, 9(1), 19374, DOI: 10.1038/s41598-019-55861-w.
- Munia, M. S., Nourani, M., Harvey, J., and Dave, H. (2023), “Interictal epileptiform discharge detection using multi-head deep convolutional neural network”, in *2023 45th Annual International Conference of the IEEE Engineering in Medicine & Biology Society (EMBC)*, IEEE, pp. 1–4, DOI: 10.1109/EMBC40787.2023.10340735.
- Nonclercq, A., and Ercek, R. (2016), “Spikedet: a spm eeg spike detection toolbox”. Available at <http://beams.ulb.ac.be/research-projects/spm-eeg-spike-detection-toolbox>.
- Nonclercq, A., Foulon, M., Verheulpen, D., De Cock, C., Buzatu, M., Mathys, P., et al. (2009), “Spike detection algorithm automatically adapted to individual patients applied to spike and wave percentage quantification”, *Neurophysiologie Clinique/Clinical Neurophysiology*, 39(2), 123–131, DOI: 10.1016/j.neucli.2008.12.001.

- Obeid, I., and Picone, J. (2016), “The temple university hospital eeg data corpus”, *Frontiers in neuroscience*, 10, 195498, DOI: 10.3389/fnins.2016.00196.
- Schmidt-Hieber, J. (2020), “Nonparametric regression using deep neural networks with ReLU activation function”, *The Annals of Statistics*, 48(4), 1875 – 1897, DOI: 10.1214/19-AOS1875.
- Smith, E. H., Liou, J.-y., Merricks, E. M., Davis, T., Thomson, K., Greger, B., et al. (2022), “Human interictal epileptiform discharges are bidirectional traveling waves echoing ictal discharges”, *Elife*, 11, e73541, DOI: 10.7554/eLife.73541.
- Thomas, J., Jin, J., Thangavel, P., Bagheri, E., Yuvaraj, R., Dauwels, J., et al. (2020), “Automated detection of interictal epileptiform discharges from scalp electroencephalograms by convolutional neural networks”, *International journal of neural systems*, 30(11), 2050030, DOI: 10.1142/S0129065720500306.
- Tjepkema-Cloostermans, M. C., de Carvalho, R. C., and van Putten, M. J. (2018), “Deep learning for detection of focal epileptiform discharges from scalp eeg recordings”, *Clinical neurophysiology*, 129(10), 2191–2196, DOI: 10.1016/j.clinph.2018.06.024.
- Torres, R. E., and Butter, I. H. (1996), “The impact of eeg technology on health manpower”, *American Journal of Electroneurodiagnostic Technology*, 36(2), 114–132, DOI: 10.1080/1086508X.1996.11080544.
- Vaswani, A., Shazeer, N., Parmar, N., Uszkoreit, J., Jones, L., Gomez, A. N., et al. (2017), “Attention is all you need”, *Advances in neural information processing systems*, 30.
- Vershynin, R. (2010), “Introduction to the non-asymptotic analysis of random matrices”, arXiv:1011.3027.

Wilson, S. B., Turner, C. A., Emerson, R. G., and Scheuer, M. L. (1999), “Spike detection ii: automatic, perception-based detection and clustering”, *Clinical neurophysiology*, 110(3), 404–411, DOI: 10.1016/s1388-2457(98)00023-6.

World Health Organization (2024), “Epilepsy”. Accessed: 2024-02-07. Available at <https://www.who.int/news-room/fact-sheets/detail/epilepsy>.

Yarotsky, D. (2017), “Error bounds for approximations with deep relu networks”, *Neural Networks*, 94, 103–114, DOI: 10.1016/j.neunet.2017.07.002.